DOI: 10.26599/FSHW.2025.9250911

Contents lists available at SciOpen

Food Science and Human Wellness

journal homepage: https://www.sciopen.com/journal/2097-0765

China Food Publishing Co.

In silico identification and biological evaluation of CXCR2 inhibitor naringin to suppress breast cancer premetastatic niche formation and metastasis

Bo Pan[a,c,1], Shengqi Wang[a,b,c,e,1], Yifeng Zheng[a,c,e], Neng Wang[d], Yingqi She[c], Shang Xu[c], Shicui Hong[c], Cheng Peng[b,*], Zhiyu Wang[a,c,e*]

[a]*State Key Laboratory of Traditional Chinese Medicine Syndrome, Chinese Medicine Guangdong Laboratory, The Second Affiliated Hospital of Guangzhou University of Chinese Medicine, Guangzhou 510006, China*

[b]*State Key Laboratory of Southwestern Chinese Medicine Resources, Chengdu University of Traditional Chinese Medicine, Chengdu, 611137, China*

[c]*Breast Disease Specialist Hospital of Guangdong Provincial Hospital of Chinese Medicine, the Second Clinical College of Guangzhou University of Chinese Medicine, Guangzhou 510006, Guangdong, China*

[d]*The Research Center for Integrative Medicine, School of Basic Medical Sciences, Guangzhou University of Chinese Medicine, Guangzhou 510006, Guangdong, China*

[e]*Guangdong Provincial Key Laboratory of Clinical Research on Traditional Chinese Medicine Syndrome, Guangdong Provincial Academy of Chinese Medical Sciences, Guangdong Provincial Hospital of Chinese Medicine, Guangzhou 510006, Guangdong, China*

ABSTRACT: Distant metastasis greatly threatens the overall survival of breast cancer patients. C-X-C chemokine receptor 2 (CXCR2) expressed on myeloid-derived suppressor cells (MDSCs) has been proven to be an essential modulator for the formation of premetastatic niche (PMN), which facilitates cancer cell seeding and later metastasis. However, current CXCR2 inhibitors are challenged by serious side effects and toxicities, thus, increasing attention has been paid to discovering CXCR2 antagonists from dietary compounds. Herein, *in silico* CXCR2 pharmacophore models were established and subsequently identified 9'''-methyl lithospermate B, thiostrepton, rhoifolin and naringin (NAR) as potential CXCR2 antagonists from the L6020 database of traditional Chinese medicine (TCM) compounds. NAR was further validated to possess the admirable target affinity with CXCR2 by BLI analysis, and DARTS detection also validated CXCR2 as the direct binding target of NAR. Further investigation revealed that NAR could suppress the metastasis of MDSC and reverse its immunosuppressive effects on $CD8^+$T cells *via* CXCR2 inhibition. Subsequent investigations utilizing the zebrafish xenotransplantation model revealed that NAR inhibited the mobilization of MDSCs and the generation of PMNs by targeting CXCR2, ultimately resulting in diminished growth and metastasis of breast cancer. Meanwhile, the mouse breast cancer orthotopic model also validated that NAR could suppress breast cancer PMN formation, growth and metastasis by inhibiting CXCR2. This suppression is evidenced by a reduction in the population of MDSCs in the lung, tumor, and blood, as well as a decrease in CXCR2 phosphorylation within splenic MDSCs. Taken together, our study identifies NAR as a natural CXCR2 antagonist, and sheds novel light on utilizing NAR to prevent PMN formation and breast cancer metastasis *via* inhibiting MDSC recruitment.

Keywords: C-X-C chemokine receptor 2; Naringin; Breast cancer; Premetastatic niche; Myeloid-derived suppressor cell;

[1]Bo Pan and Shengqi Wang contributed equally to this work.
***Corresponding author**
pengchengchengdu@126.com; wangzhiyu@gzucm.edu.cn

Received 5 July 2025
Received in revised from 1 August 2025
Accepted 28 September 2025

1. Introduction

Breast cancer has become the leading female malignancy, with the highest incidence of 23.8% and mortality rates of 15.4% worldwide in 2022 [1]. As a clinically heterogeneous disease, distant metastasis remains the greatest threat to the prolonged survival of breast cancer patients, although substantial progress has been made in its diagnostic methodologies and therapeutic strategies. Research data have revealed that the long-term survival rate of metastatic breast cancer was less than 5% [2], and 6% of patients were identified with metastasis at the first diagnosis. Moreover, up to 50% of breast cancer patients developed distant metastasis within three years [3]. Therefore, advancing therapeutic strategies for inhibiting breast cancer metastasis and developing novel targeted drugs is an urgent task for oncologists globally.

Premetastatic niche (PMN) is based on the "Seed and soil" theory proposed in 1889 by Stephen Paget, where metastatic cancer cells and premetastatic sites were demonstrated as "seed" and "soil", respectively. It was first reported by Kaplan et al. in 2005 that cellular factors such as vascular endothelial growth factor (VEGF) and placental growth factor (PLGF), secreted by primary tumors, facilitate the recruitment of bone marrow-derived hematopoietic progenitor cells to tumor-specific pre-metastatic sites, then develop an immunosuppression microenvironment prior to the metastasis of cancer cells [4]. Studies in recent years have discovered that PMN is created to promote an immunosuppressive microenvironment in pre-metastatic organs, thereby facilitating the subsequent seeding of cancer cells [5]. It has been proven that during the formation of PMN, various immunosuppressive cells, such as metastasis-associated macrophages (MAMs), regulatory T cells (Tregs) and myeloid-derived suppressor cells (MDSCs), were recruited to the targeted metastatic organs [6]. MDSCs are a class of heterogeneous cells that possess immunosuppressive properties and are involved in PMN formation and cancer metastasis [7]. MDSCs are characterized by granulocytic markers of CD11b and Ly6G, and their immunosuppressive abilities are generally regulated through C-X-C chemokine receptor 2 (CXCR2), C-C chemokine receptor type 5 (CCR5) and colony-stimulating factor 1 receptor (CSF-1R) [8]. Chemokines secreted by malignancies, such as CXCL1, CXCL2 and S100A8/9, play crucial roles in mobilizing MDSCs to pre-metastatic organs during the process of PMN formation [9]. MDSCs have been proven to support an immunosuppressive tumor immune microenvironment (TIME) *via* hindering the infiltration and multiplication of $CD3^+/CD8^+$ T cells, accompanied by the accelerated differentiation of Tregs and inhibition of cytotoxic NK cells [10].

CXCR2, expressed on MDSCs, is the receptor for seven kinds of CXC chemokines, including CXCL1 [11]. In carcinogenesis and subsequent progression, CXCR2 was reported to participate in the recruitment of MDSCs to primary tumors and exert immunosuppressive effects [12]. Besides, $CXCR2^+$MDSCs were also found to participate in PMN establishment by interacting with CXCL1. Consequently, blocking of CXCL1/CXCR2 interaction by CXCR2 inhibitors significantly reversed the suppression of MDSCs on the cytotoxic killing effects of NK cells, thereby inhibiting cancer progression and metastasis [13]. More importantly, clinical studies revealed that high levels of CXCR2 and CXCL1 predicted poor prognosis in lung and colon cancer [14, 15], and the elevated expression of CXCL1 is correlated with increased MDSC infiltration

in ovarian cancer patients [16]. In particular, although triple-negative breast cancer (TNBC) shows elevated levels of tumor-infiltrating lymphocytes (TILs) compared to non-TNBC, and immunotherapy has demonstrated efficacy in prolonging overall survival, it was discovered that tumor samples of TNBC patients exhibited elevated CXCR2 expression compared to those of non-TNBC patients, leading to higher levels of MDSC infiltration [17, 18]. Moreover, only approximately 23% of PD-L1-positive TNBC patients responded to immune checkpoint inhibitors [18]. Therefore, switching therapeutic targets from $CD8^+$ T cells to immunosuppressive cells by targeting CXCR2 might be another approach for TIME remodeling and PMN prevention.

Apart from siRNA and neutralizing antibodies, small-molecule inhibitors are the most commonly applied antagonists for CXCR2, and over a dozen distinct classes have been developed since the first antagonist, SB225002, was discovered in 1998 [19, 20]. In recent years, several CXCR2 antagonists, such as reparixin, have undergone clinical trials for metastatic cancer treatments [21]. However, these synthetic CXCR2 antagonists might bring severe side effects including neutropenia induced by agents such as navarixin or AZD5069, and airway inflammation caused by SB656933 [22, 23], which greatly hinder their clinical applications. Conversely, natural dietary compounds have garnered heightened interest for their role in facilitating cancer treatment, owing to their low toxicity and minimal adverse effects. [24-26]. Therefore, developing antagonists from dietary compounds with moderate inhibitory effects and low toxicity may lead to the discovery of novel drugs against CXCR2. Typically, conventional pharmacological screening strategies require establishing cellular models, which is time-consuming and costly. By contrast, an *in silico* screening technique combined with pharmacological validation provides a high-throughput screening strategy to optimize screening efficiency and maintain the target-specific properties of candidate compounds [27]. In recent years, computer-aided screening methods have successfully assisted in discovering active ingredients against Zika virus and COVID-19 infections, as well as gallbladder cancer [24, 28, 29].

Herein, ligand-based pharmacophore models were established to screen potential CXCR2 inhibitors from a natural compound library. It was found that naringin (NAR) could directly bind to CXCR2, thereby inhibiting its phosphorylation and the activation of downstream STAT3 signaling. The *in vivo* study revealed that NAR exhibited inhibitory effects on breast cancer PMN formation and metastasis by preventing MDSC mobilization through CXCR2 suppression. Our study provided NAR as a natural CXCR2 inhibitor and highlighted its pharmacologic activity in inhibiting PMN formation and MDSC mobilization.

2. Materials and methods

2.1 Cell culture and induction

Human Embryonic Kidney 293 cell line (HEK293) and mouse TNBC cell line (4T1) were acquired from the American Type Culture Collection (ATCC). Luciferase gene-tagged 4T1 (4T1-Luc) cells were generated following the instructions of our previous report [30]. All cell lines were propagated in the DMEM medium supplemented with 10% fetal bovine serum (FBS) and 1% penicillin-streptomycin antibiotic mixture, and were maintained in standard culture conditions of 37℃ and 5% CO_2 in a humidified incubator. Chemical

compounds applied for *in vitro* investigation were dissolved and stored in DMSO at a concentration of 10 mmol/L. To evaluate the phosphorylation of CXCR2 and the downstream STAT3, HEK293 cells were treated with NAR or SB225002 for 1.5 h. To analyze the mRNA expression of STAT3-related cytokines, cells were treated with NAR for 48 h. To investigate influences of NAR on MDSCs, MDSCs were pre-treated with NAR for 24 h before further investigations.

2.2 Establishment of ligand-based pharmacophore models and virtual screening in the L6020 database

The structures and IC_{50} values of each chemical compound with CXCR2 inhibitory properties were collected from the literature [31-36], and Discovery Studio 2016 (BIOvia, San Diego, USA) was applied to establish the HipHop and Hypogen pharmacophore models. The parameters for establishing the HipHop and Hypogen pharmacophore models were based on previous reports with slight modifications [37, 38]. The L6020 database of traditional Chinese medicine (TCM) compounds was provided by Topscience (Shanghai, China), which was converted into a 3D structure database with Discovery Studio 2016 software. For the selection of potential CXCR2 antagonists, the estimated (Est) IC_{50} cut-off point of the Hypogen model was set at 1 μmol/L, and the Fit value cut-off point of the HipHop model was set at 2.

2.3 Molecular docking and dynamics simulation assay

Molecular docking of potential CXCR2 antagonists was performed with Discovery Studio 2016. Briefly, CXCR2 protein (PDB id: 8XX6) was optimized and the active site was determined at the binding site of IL-8/CXCR2. Subsequently, potential CXCR2 antagonists were docked to CXCR2 protein using Flexible docking protocol. Molecular dynamics simulation was performed with AMBER 22 software (University of California, Los Angeles, USA), all simulations were performed using pmemd program to simulate a 50 ns interaction between small molecule and CXCR2, the Root-Mean-Square Deviation (RMSD) and Root-Mean-Square Fluctuation (RMSF) of small molecule in complex with CXCR2 were recorded.

2.4 Biolayer interferometry (BLI) assay

CXCR2 protein was purchased from Crystalo Biopharma (Shenzhen, China), and was then biotinylated with a Biotinylation Kit (BMD Labservice, Jiangsu, China) before being immobilized on the biosensors of OctetRed96 (Pall ForteBio Corp., Garten City, USA). Subsequently, the biosensors were treated with compounds screened from the L6020 database at a concentration of 100 μmol/L to detect the kinetic response signal of the thickness changes of the sensor layer reflecting the affinities of compounds for CXCR2. Rhoifolin, 9'''-methyl lithospermate B, eriocitrin, lithospermic acid, NAR, and thiostrepton (Purity ≥ 98%) were purchased from Selleck Chemicals (Houston, USA). Massoniresinol, debenzoylgalloylpaeoniflorin, and forsythoside F were purchased from Yuanye Bio-Technology (Shanghai, China). For the analysis of the Steady State KD (SSKD), compounds with positive kinetic response were dissolved to various concentrations ranging from 1 μmol/L to 100 μmol/L, and the kinetic response of every concentration was measured for steady-state analysis performed on the Octet RED User Software to obtain SSKD of each compound.

2.5 Drug Affinity Responsive Target Stability (DARTS) assay

DARTS assay was designed according to the procedure of the previous protocol [39]. Briefly, varied concentrations of NAR (1–10 μmol/L) and 1 μmol/L SB225002 (Selleck Chemicals, Houston, USA) were administered to HEK293 cells for 3 h. Then the collected cells were lysed with RIPA (Beyotime, Jiangsu, China) and further treated with 0.05mg/mL protease (Roche Diagnostics, Indianapolis, USA) for another 30 min. The protein samples were collected and loaded onto SDS-PAGE. Coomassie blue staining assay was applied to visualize the differential protein bands. Target gel bands of interest were cut out, lysed and enzymatically digested for subsequent mass spectrometry characterization.

2.6 Western blot assay

HEK293 cells were treated with thiostrepton, Rhoifolin, 9'''-methyl lithospermate B, NAR, and SB225002, respectively. Then, cells treated with the indicated compounds were lysed using RIPA, and subsequently centrifuged at 12000 r/min for 10 min to remove cell debris, the total protein content in the cellular lysates was quantified using the bicinchoninic acid (BCA) protein assay to normalize protein loading across each group. After thermal denaturation, 30 μg of total protein per sample was loaded and separated *via* SDS-PAGE, protein fractions were then systematically electrotransferred onto polyvinylidene fluoride (PVDF) microporous membranes (Millipore, Bedford, USA). After incubating with primary antibodies overnight, immunoblotted membranes were further probed with horseradish peroxidase (HRP)-conjugated secondary antibodies for 1 h. Finally, ECL Advance reagent (Tanon Science & Technology, Shanghai, China) was applied to image protein bands of each group. The primary antibodies for p-STAT3 (9145T), STAT3 (4904T), β-actin (4970S), and GAPDH (5174T) were purchased from Cell Signaling Technology (Danvers, USA). The primary antibody for CXCR2 was purchased from Proteintech (20634-1-AP, Chicago, USA), and p-CXCR2 antibody was purchased from Cohesion Biosciences (CPA4620, London, UK). Secondary antibodies were purchased from Cell Signaling Technology (7074S, Danvers, USA).

2.7 pcDNA3.4-CXCR2 plasmid transfection

For plasmid transfection, the pcDNA3.4-CXCR2 plasmid and the Vigene Fection Kit were purchased from Vigene Biosciences (Jinan, China). HEK293 cells were transfected with the plasmid using the Vigene Fection kit following the manufacturer's protocol. The protein expression after transfection was assessed by Western blot analysis.

2.8 Preparation of MDSCs and CD8+ T cells

MDSCs and $CD8^+$ T cells were isolated from murine bone marrow and spleen tissues, respectively. Cells flushed out from the bone marrow were incubated with CD45 (25-0451-82, Thermo Fisher Scientific, Waltham, USA), CD11b (101208, Biolegend, San Diego, CA, USA), and Gr-1 (108406, Biolegend, San Diego, USA) antibodies for the detection of MDSCs. Cells obtained from the spleen were stained with CD3 (100204, Biolegend, San Diego, USA) and CD8 antibodies (100417, Biolegend, San Diego, USA) for the detection of $CD8^+$ T cells. Subsequently, cells were isolated through fluorescence-activated cell sorting (FACS). MDSCs applied in the co-culture system were pretreated with 10 ng/mL CXCL1 for 24 h. For the

stimulation of $CD8^+$ T cells, the sorted cells were further incubated with 50 ng/mL PMA, 1 μg/mL ionomycin, and 10 ng/mL IL-2 (Multiscience, Hangzhou, China) for 24 h before further investigations.

2.9 Cell proliferation detection.

To analyze the proliferation of 4T1 co-cultured with MDSCs, the conditioned medium of MDSCs (MDSC-CM) pretreated with CXCL1 and NAR was collected and administrated to 4T1 cells for 24 h, the cell proliferation of 4T1 was detected with a CCK-8 kit (Beyotime, Jiangsu, China) following the same instruction as a previous report [40].

2.10 Flow cytometry assay

For the detection of cell apoptosis, 4T1 cells were labeled with Annexin V-FITC and propidium iodide reagent (KeyGEN Biotech, Jiangsu, China) and the apoptosis ratio of 4T1 cells was detected by flow cytometry. To perform the carboxyfluorescein succinimidyl ester (CFSE) assay, $CD8^+$ T cells were stained with CFSE reagent (Beyotime, Jiangsu, China) before being co-cultured with MDSCs. After co-culturing for 24 h, CFSE distribution in $CD8^+$ T cells was evaluated *via* flow cytometry. For the detection of perforin expression of $CD8^+$ T cells, cells in the MDSCs/$CD8^+$ T co-cultured system were incubated with CD8 and perforin antibodies (12-9392-82, Thermo Fisher Scientific, Waltham, USA). The population of perforin-positive cells in $CD8^+$ T lymphocytes was further detected by flow cytometry.

2.11 Wound healing and transwell assay

To assess the influence of NAR on 4T1 migrations, 4T1 cells were treated with MDSC-CM collected in 2.9 for 24 h, and subsequent wound healing and transwell assay were conducted following previous studies [41, 42]. To assess the mobilization capacity of MDSCs under different treatments, a transwell system was established according to our previous report [43]. The penetrated MDSCs from the upper chambers were examined by Coomassie Blue staining, and the area of cells from the upper chambers passing through the membrane was measured.

2.12 Zebrafish xenotransplantation model of breast cancer

AB strain zebrafish were obtained from the China Zebrafish Resource Center (Wuhan, China). The embryotoxicity assay of NAR was performed following the protocol of our previous report [30]. Zebrafish larvae within 24 h post-hatching were employed in pharmacological studies, since their immune system was not yet fully developed. To evaluate the effect of CXCL1 on the metastasis of MDSC, Dio-stained MDSCs were pre-treated with varied concentrations of CXCL1 and then microinjected into the subintestinal vasculature of zebrafish. Subsequently, the MDSC-bearing zebrafish were further incubated with or without SB225002 for 12 h and observed under a fluorescence microscope (Nikon Eclipse C1, Tokyo, Japan). To observe the effect of MDSCs on 4T1 metastasis and the inhibitory effect of NAR, CXCL1-treated MDSCs were injected into zebrafish as described above. Zebrafish were then treated with or without NAR (1-5 μmol/L) for 12 h, followed by the injection of 4T1 cells. Zebrafish were transferred to a NAR-free environment for an additional 3 h, and MDSCs/4T1 metastasis were observed under a fluorescence

microscope. To investigate the immunosuppressive effect of MDSCs on $CD8^+$ T cells and the reversal exerted by NAR, CXCL1-treated WT/CXCR2-KO MDSCs, 4T1cells, and $CD8^+$ T cells were co-injected into zebrafish, which were further incubated with or without NAR for 48 h. The proliferation and metastasis of 4T1 cells were subsequently observed under a fluorescence microscope.

2.13 QPCR assay

For the extraction of total RNA from HEK293 cells or from blood samples of mice, HEK293 cells were digested and centrifuged at 500 g for 5 min, while blood samples were centrifuged at 1500g for 15 min following red blood cells lysis. Then the total RNA was extracted with an EASYspin Plus RNAiso kit (Aidlab Bio, Beijing, China) according to the manufacturer's instructions. Total RNA was transcribed into complementary cDNA using the PrimeScript™ RT reagent kit with a gDNA eraser (Takara BIO, Kyoto, Japan). The QPCR experiment was performed using the SYBR® Premix Ex TaqTM II kit (Takara BIO, Kyoto, Japan) on the Applied Biosystems ViiA7 Real-Time PCR System (Thermo Fisher Scientific, Waltham, USA). The primer sequences were GCCTAACATGCTTCGAGATC (Forward) and TGATGTCTGGGTCTTGGTTC (Reverse) for human IL-10, AAGGAGGAGGGCAGAATCAT (Forward) and AAGGAGGAGGGCAGAATCAT (Reverse) for human VEGF, GCATCCCCCAAAGTTCACAA (Forward) and AGGACTGGGCCATTCTCCTT (Reverse) for human β-actin. Meanwhile, the primer sequences were GCTCAGCAAGGAGGTAGGTG (Forward) and TCTTACCGGTGTCCAAGTCC (Reverse) for mouse Luciferase, and GTGTGCACTTTTATTGGTCTCAA (Forward) and GGAGGGGGTTGAGGTGTT (Reverse) for mouse β-actin. The relative mRNA levels were compared using the $2^{-\Delta\Delta Ct}$ method.

2.14 Immunofluorescence analysis

The lung specimens were fixed and sliced following the procedures of our previous report [43]. Tissue sections were incubated with PE-Cy7-conjugated CD11b, FITC-conjugated Gr-1 and CK19 (10712-1-AP, Proteintech, Chicago, USA) antibodies overnight, and further incubated with Alexa Fluor® 555-conjugated anti-rabbit IgG (4413S, CST, Danvers, USA) to label CK19 for 2 h. Spleen-derived MDSCs were incubated with the p-CXCR2 antibody overnight, and further incubated with Alexa Fluor® 555-conjugated anti-rabbit IgG. Fluorescence images were taken under the LMS710 Confocal Microscope (ZEISS, Jena, Germany).

2.15 Animal experiment

All animal experiments were performed following the experimental protocols approved by the Institutional Animal Care and Use Committee at Guangdong Provincial Hospital of Chinese Medicine (ethics approval number: 2019061). Female 9-week-old Balb/c mice were purchased from Vital River Laboratory Animal Technology (Beijing, China), and Balb/c genetic background CXCR2-knockout (CXCR2-KO) mice were obtained from Gempharmatech (Nanjing, China). Mice were housed under pathogen-free conditions in the Experimental Animal Center of Guangdong Provincial Hospital of Chinese Medicine and supplied with sterilized food and water. 2×10^6 4T1-Luc cells in 200 μL PBS were injected into

the mammary fat pads of mice to establish an *in vivo* breast cancer model. Animals were divided into four groups (n = 15), including the saline group, 10 mg/kg/d NAR group, 25 mg/kg/d NAR group and 2 mg/kg/d SB225002 group. All drugs were administered by intraperitoneal injection. The tumor size and body weight were measured every three days, and tumor volumes (V) were calculated with the formula: $V = (\text{length}) \times (\text{width})^2/2$. D-luciferin (PerkinElmer, Boston, USA) was intraperitoneally injected into mice, and the luminescent images were taken under the IVIS Spectrum system (PerkinElmer, Boston, USA) to monitor lung metastasis in mice. After six weeks, mice were anesthetized using intraperitoneal injection of sodium pentobarbital, and the tumor, lung and spleen tissues were removed. MDSCs proportions were detected in tumor, lung tissue and blood samples using flow cytometry as described above. Moreover, from the 2nd to the 4th week, MDSC proportions in the tumor, blood, and lung were also detected.

2.16 Hematoxylin and eosin (HE) staining analysis

The lung tissues of tumor-bearing mice were fixed and sliced as described above. HE staining was conducted with hematoxylin and eosin dyes (Beyotime, Jiangsu, China) following instructions from the manufacturer.

2.17 Statistical analyses

Statistical analyses were performed with SPSS software (IBM SPSS Statistics, version 26.0). Data are presented as the mean ± standard deviation (SD). One-way analysis of variance (ANOVA) and Student's t-test were applied. For dose-dependent comparisons, the Dunnett post hoc test was applied, while the Bonferroni method was used for the remaining comparisons. Repeated-measures ANOVA was used to analyze repeated-measurement data. Statistical significance was defined at $P < 0.05$.

3. Results

3.1 Identification of potential CXCR2 antagonists through the Hypogen and HipHop pharmacophore models

To identify candidate inhibitors targeting CXCR2, two ligand-based computer-aided pharmacophore models were established for the screening from the L6020 database (**Fig. 1A**), which contains 15,000 natural compounds. For the establishment of the Hypogen pharmacophore model, four classes (squaramides, guanidines, diarylureas, and tetrahydrobenzothiophene) of 40 compounds (**Fig. S1A** and **Table S1–2**) with known CXCR2 inhibitory activity were classified into active, moderately active and inactive compounds according to their inhibitory abilities (IC_{50}), and then randomly allocated into the training and test sets. Common features of the Hypogen model were generated based on the structures of the two highest-activity compounds in the training set and were further modified and pruned based on the structures of the remaining moderately active and inactive compounds. A total of 10 pharmacophore models were generated after processing the 3D QSAR pharmacophore generation. The Null Cost Distance of Hypo-1 and Hypo-2 were 71.928 and 67.354, respectively (**Table S3**). The best pharmacophore hypothesis was Hypo-1 (**Fig. 1B**), which possessed two hydrogen-bond acceptors (HBA), two hydrogen-bond donors (HBD), one hydrophobic group (HYD) and two ring aromatic groups (RA). Hypo-1 also showed the highest correlation in the training

set (**Fig. S1B**). To verify the reliability of Hypo-1, the ligand profile verification protocol was performed on the test set. As shown in **Fig. S1C**, Hypo-1 presented admirable linear regression in Fit value, which was closely related to the inhibitory ability of compounds in the test set. Subsequently, the Hypogen pharmacophore model of Hypo-1 was applied in the screening from the L6020 database, and the top 10 compounds with CXCR2 inhibitory activity were presented in **Fig. 1C**. The predicted IC_{50} values of these compounds were less than 1 μmol/L, and the best one was identified as thiostrepton with an IC_{50} of 0.133646 μmol/L.

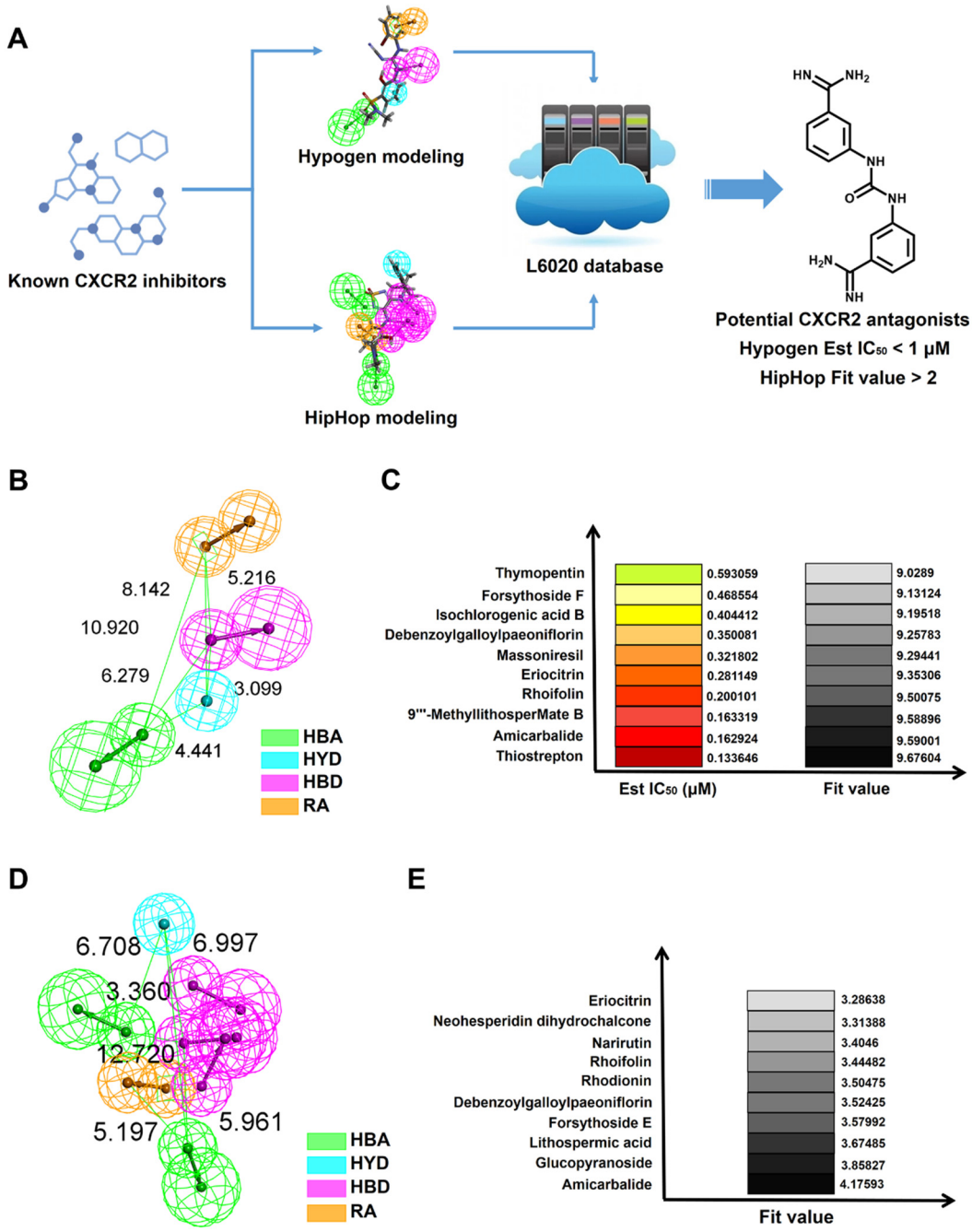

Fig. 1 Pharmacophore models of Hypogen and HipHop. (A) The screening strategy for potential CXCR2 antagonists from the L6020 database. **(B)** Pharmacophore features of the best hypothesis model Hypo-1 generated in Hypogen are shown in green for hydrogen-bond acceptor (HBA), magenta for hydrogen-bond donor (HBD), cyan for hydrophobic group (HYD), and orange for ring aromatic group (RA). **(C)** The top 10 compounds screened by the Hypo-1 Hypogen model from the L6020 database. **(D)** The pharmacophore features of the best hypothesis model Hypo-4. **(E)** The top 10 compounds screened by the Hypo-4 HipHop model from the L6020 database.

To optimize the above results, another ligand-based pharmacophore model of HipHop was established. The structures of selected compounds in the training set were shown in **Fig. S1D**. After the Common Feature Pharmacophore Generation protocol was performed, Hypo-4 was determined as the most suitable model (**Fig. 1D**), which possessed four HBA, six HBD, one HYD, and two RA. Subsequently, Hypo-4 was verified to present the best selectivity to identify the known CXCR2 inhibitors in a test set that consisted of six CXCR2 inhibitors and 17 non-inhibitory compounds (**Fig. S1E**). Therefore, Hypo-4 was applied for CXCR2 inhibitor screening from the L6020 database, in which the fit value cut-off was set at 2.0. The top 10 compounds with potential CXCR2 inhibitory activities were presented in **Fig.1E**. These compounds fit well in the Hypo-4 model with a fit value higher than 3.0, and amicarbalide was identified with the highest fit value of 4.17593.

3.2 Affinity evaluation of potential CXCR2 inhibitors

By intersecting the compounds screened by Hypogen and HipHop, the top 15 candidate inhibitors with IC_{50} less than 1 μmol/L and HipHop Fit value higher than 2.0 were identified (**Fig. S2**). Following toxicity and druggability assessments based on literature research [44-46], five compounds were ruled out from further consideration based on their potential toxicity and unsatisfactory stability, and the rest 10 compounds with promising biocompatible properties were selected for further investigations (**Fig. 2A**). To ascertain the affinity of these compounds for CXCR2, we conducted molecular docking studies to elucidate their interactions. The results indicated that nine out of ten compounds were docked within the IL-8 binding site of CXCR2, exhibiting negative CDock energies. This outcome suggested that these small molecules possess the capability to bind effectively to CXCR2, as depicted in **Fig. S3A-B**. To validate the above finding, the BLI assay was further applied. The biotinylated CXCR2 protein was successfully immobilized to the biosensors and subjected to detection. Four compounds including 9'''-methyl lithospermate B, thiostrepton, rhoifolin, NAR and the positive CXCR2 inhibitor SB225002 were finally found to present positive responses for CXCR2 binding (**Fig. 2B–C**). Furthermore, the molecular dynamics simulation outcomes substantiated that the four compounds formed a stable complex with CXCR2 within 30 ns **(Figure S3C**), exhibiting minimal residue fluctuation in contrast to the unbound protein (**Figure S3D**). Each of these compounds established a minimum of four to five stable hydrogen bonds with CXCR2 residues **(Figure S3E**), signifying their robust affinity for CXCR2. In order to estimate the binding affinity of these four compounds to CXCR2, the Steady State KD (SSKD) was measured by BLI. SSKD values of 9'''-methyl lithospermate B**,** thiostrepton, rhoifolin, NAR and the positive inhibitor SB225002 were $1.9e^{-4}$, $7.9e^{-8}$, $6.5e^{-5}$, $2.9e^{-5}$ and $1.4e^{-7}$ (**Fig. 2D** and **Fig. S4A–E**), respectively. Taken together, thiostrepton presents the lowest SSKD, indicating its highest binding ability with the CXCR2 protein.

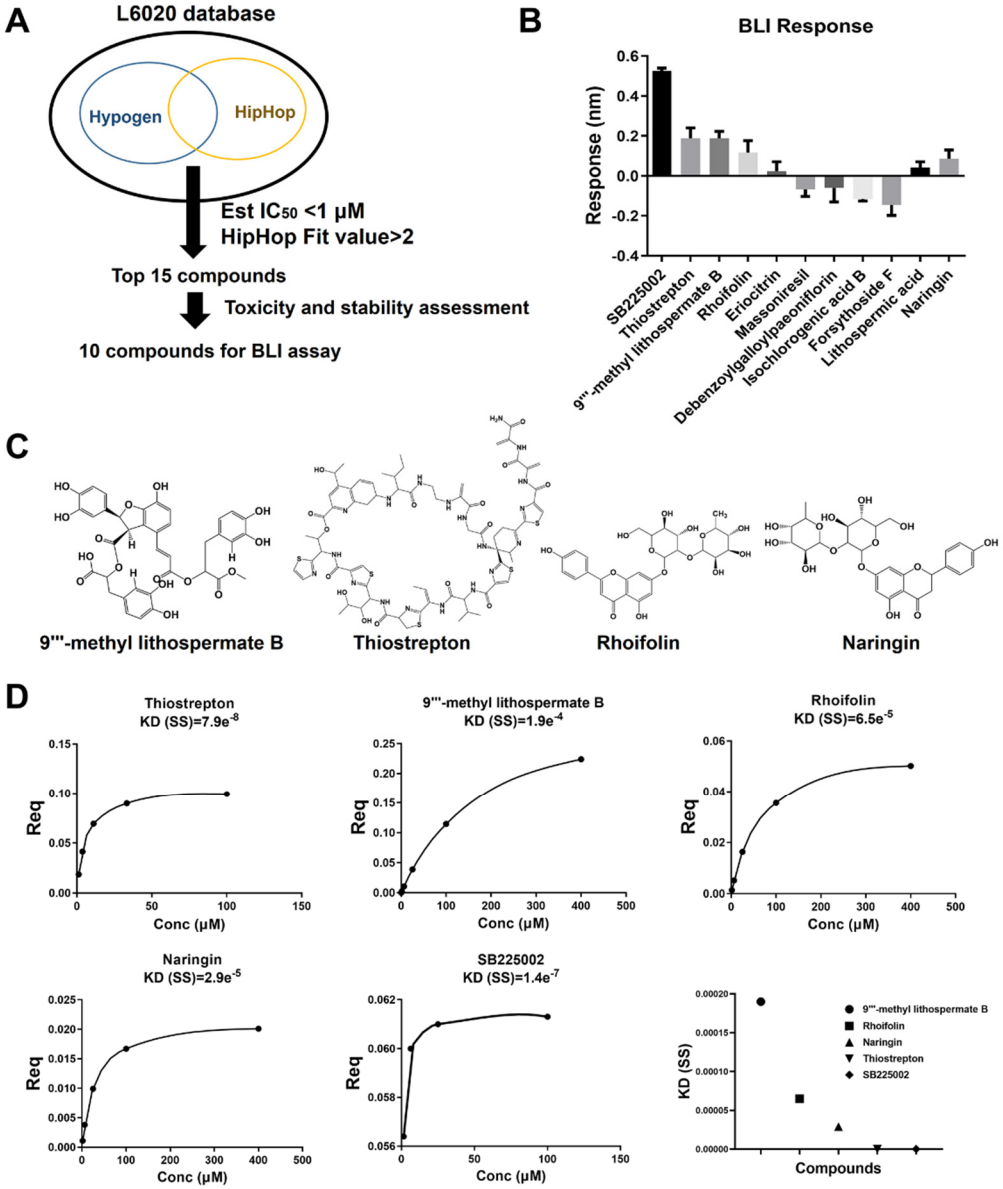

Fig. 2 Biolayer interferometry assay (BLI) for CXCR2 binding study. (A) The strategy for compound assessments from the L6020 database to perform a BLI assay. **(B)** BLI screening of the top 10 active compounds screened by HipHop and Hypogen pharmacophore models. The applied concentration of chemical compounds was 100 μmol/L. n = 3. **(C)** Chemical structures of compounds with positive BLI response. **(D)** Steady State (SS) analysis of thiostrepton, 9'''-methyl lithospermate B, rhoifolin, naringin, and SB225002. Req refers to the response in equilibrium.

3.3 Identification of NAR as a CXCR2 inhibitor by the DARTS assay

Based on the results of the BLI assay, the effects of 9'''-methyl lithospermate B, thiostrepton, rhoifolin, and NAR on the phosphorylation of CXCR2 were measured by Western blot. CXCR2 phosphorylation occurred shortly after binding with its ligands [47]. Following treatment for 1.5 h, the phosphorylated CXCR2 of HEK293 cells treated with NAR was significantly downregulated dose-dependently and presented a higher inhibition ratio compared to the other three compounds (**Fig. 3A**). This result revealed that NAR presented a similar inhibitory effect as SB225002 to block the interaction between CXCR2 and its ligands, and further investigations were proceeded to verify the CXCR2 targeting ability of NAR. DARTS is a reliable strategy developed to identify the intracellular target of phytochemicals based on the decreased proteolysis after binding with the target protein, resulting in the appearance of gradually enhanced band

intensity with the increasing concentration of pronase. The protein band was then dissected and subjected to LC-MS identification (**Fig. 3B**). The result of the DARTS assay revealed that after pronase treatment, the proteolysis of protein bands between 40 kDa and 55 kDa was inhibited by SB225002 and NAR dose-dependently (**Fig. 3C**). The protein bands were then lysed and analyzed by LC-MS. The first-order spectrum and the second-order spectrum of samples treated by NAR and SB225002 were shown in **Fig. 3D** and **Fig. 3E**, and were finally identified as CXCR2. These findings suggest that NAR is a natural CXCR2 inhibitor.

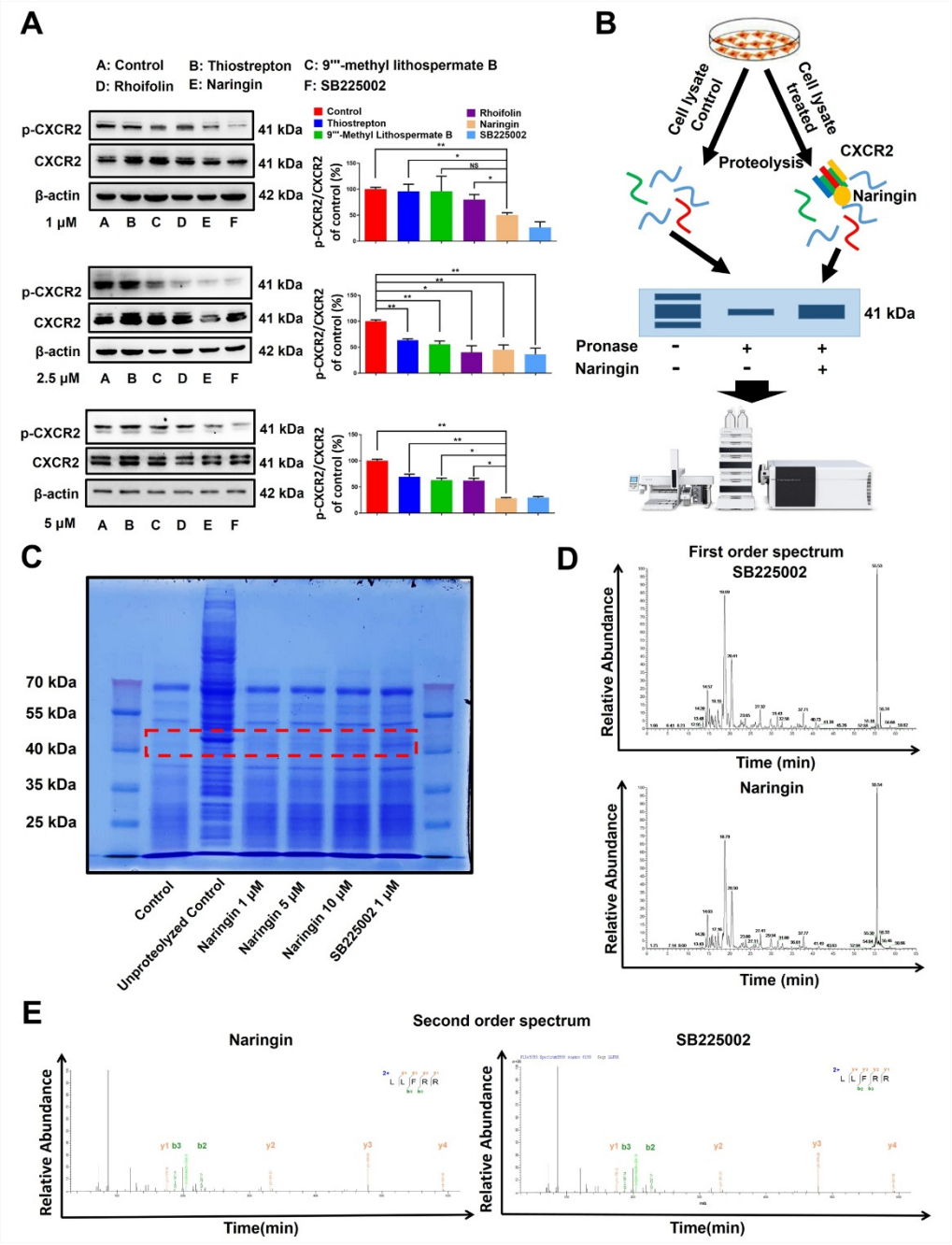

Fig. 3 NAR inhibited CXCR2 phosphorylation. (A) The effect of potential antagonists on CXCR2 phosphorylation. HEK293 cells were treated with thiostrepton, 9'''-methyl lithospermate B, rhoifolin, and NAR at 1 μmol/L, 2.5 μmol/L, and 5 μmol/L for 1.5 h, respectively. SB225002 was administered at 1 μmol/L. The optical intensity of Western blot bands was measured. n = 3/group. **(B)** The experimental strategy of DARTS. **(C)** The Coomassie blue staining of SDS-PAGE loaded with HEK293 cell lysates. **(D)** First-order mass spectrograms of positive protein bands responsive to NAR and SB225002. **(E)** Second-order mass spectrograms of positive protein bands responsive to NAR and SB225002. CXCR2 peptide fragments were detected. Data are presented as mean ± SD, $^{*}P < 0.05$, $^{**}P < 0.01$.

3.4 NAR inhibits the downstream STAT3 phosphorylation by targeting CXCR2

Since STAT3 is known to be a downstream signaling molecule of CXCR2 [48], the effect of NAR on STAT3 phosphorylation is further investigated. First, we confirmed that NAR possessed inhibitory activity on CXCR2 phosphorylation in HEK293 cells in a dose-dependent manner **(Fig. 4A)**. Subsequently, STAT3 phosphorylation in HEK293 cells was also inhibited by NAR dose-dependently **(Fig. 4B)**, indicating that NAR might inhibit STAT3 phosphorylation by targeting CXCR2. To validate the hypothesis, CXCR2 was overexpressed in HEK293 cells. As shown in **Fig. 4C**, the level of phosphorylated CXCR2 was dramatically elevated following CXCR2 overexpression. Notably, the phosphorylated STAT3 and the ratio of p-STAT3/STAT3 were dramatically increased **(Fig. 4D)**, indicating that STAT3 is actually a downstream signaling molecule of CXCR2. Moreover, the inhibitory effects of NAR on both CXCR2 and STAT3 phosphorylation were significantly relieved following CXCR2 overexpression **(Fig. 4E–F)**, suggesting that CXCR2 plays a crucial role in mediating the pharmacological activity of NAR. To further investigate the influence of NAR on STAT3-regulated cytokines, we analyzed the expression of VEGF and IL-10, both are highly associated to PMN formation [49], and found that gene expressions of VEGF and IL-10 were subsequently suppressed by NAR in a dose-dependent manner (**Fig. S5A–B**). Taken together, the above findings suggested that NAR exerted potential to suppress PMN formation *via* inhibiting CXCR2 and the down-stream signaling.

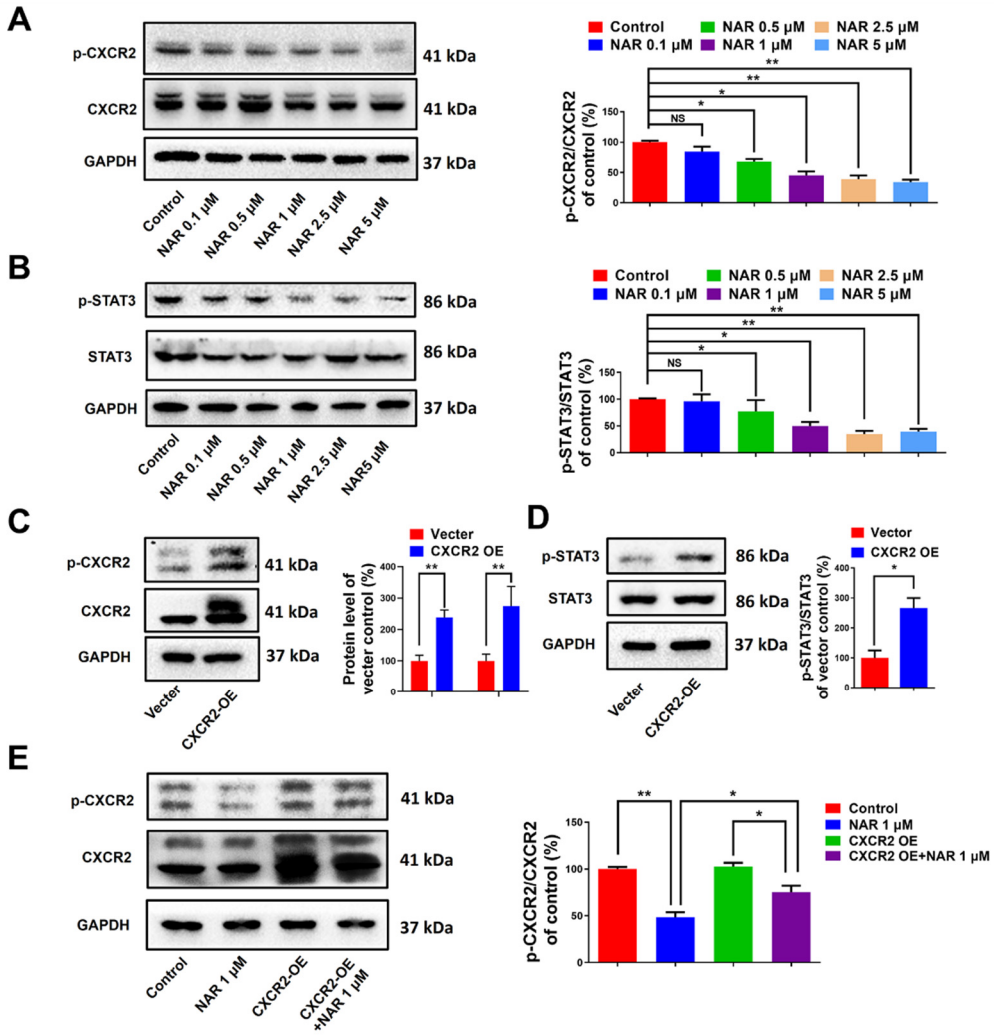

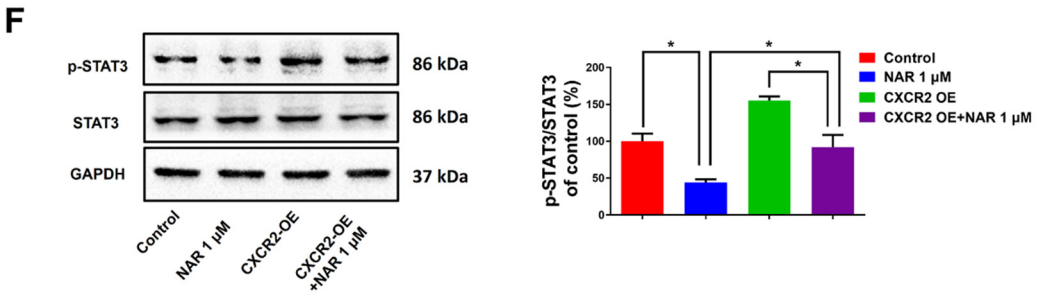

Fig. 4 NAR inhibited CXCR2 phosphorylation and downstream STAT3 phosphorylation. (A) NAR inhibited CXCR2 phosphorylation in a dose-dependent manner. **(B)** NAR inhibited STAT3 phosphorylation in a dose-dependent manner. **(C)** CXCR2 phosphorylation level was markedly elevated after the transfection of CXCR2 overexpression (OE) plasmids into HEK293 cells. **(D)** STAT3 phosphorylation level was markedly activated after CXCR2 overexpression. **(E)** The inhibition of CXCR2 phosphorylation by NAR was reversed by CXCR2 overexpression. **(F)** The inhibition of STAT3 phosphorylation by NAR was reversed by CXCR2 overexpression. Data are presented as mean ± SD, n = 3, $^{*}P < 0.05$, $^{**}P < 0.01$.

3.5 NAR inhibits the recruitment and immunosuppressive effect of MDSC via CXCR2

MDSCs are known to present a significant immunosuppressive effect in TNBC, and CXCR2 is involved in MDSC recruitment, infiltration, and immunosuppression. Herein, we acquired bone marrow-derived MDSCs from the bone marrow of Balb/c mice through FACS **(Fig. 5A)**. Chemokine CXCL1 is one of the CXCR2 ligands and is proven to promote MDSC metastasis and immunosuppression [50]. It was observed that the invasion ability of MDSCs in the transwell system was markedly increased under CXCL1 treatment and dose-dependently inhibited by NAR treatment **(Fig. 5B)**. The immunosuppressive property of MDSCs was also investigated by co-culturing with $CD8^+$ T cells derived from mouse spleens **(Fig. 5C)**. The result of CFSE analysis revealed that the proliferation rate of $CD8^+$ T cells was dramatically decreased after co-culture with CXCL1-treated MDSCs at a 2:1 ratio, and this effect was markedly reversed by NAR treatment in a dose-dependent manner **(Fig. 5D)**. Apart from detecting cell division activity, the suppression effect of CXCL1-treated MDSCs on perforin secretion from $CD8^+$ T cells was also markedly reversed following NAR treatment dose-dependently **(Fig. 5E)**. To determine the influence of NAR on the cytotoxic effects of $CD8^+$ T cells against cancer cells, a $CD8^+$ T/MDSC/4T1 co-culture system was further established, the ratio of $CD8^+$T, MDSC and 4T1 was set as 5:2.5:1. MDSCs were firstly treated with CXCL1 or NAR for 24 h, the live MDSCs were then washed to deplete CXCL1 or NAR, and then co-cultured with $CD8^+$ T and 4T1 breast cancer cells. After 24 h, the apoptosis rate of 4T1 cells was measured by flow cytometry. The result showed that after co-culture with $CD8^+$ T cells, the apoptosis rate of 4T1 cells was significantly increased, but reduced when MDSCs were administered. Notably, when NAR-treated MDSCs were added, the apoptosis rate of 4T1 cells was then dose-dependently increased, indicating that the cytotoxic effects of $CD8^+$ T were recovered due to the suppressed MDSC activity by NAR **(Fig. 5F)**. During PMN formation, MDSC also facilitates tumor progression [49]. In addition, we discovered that MDSCs significantly promoted 4T1 proliferation and migration, which were markedly suppressed by NAR treatment **(Fig. S5C–D)**. These findings suggest that NAR could inhibit the recruitment and immunosuppressive abilities of MDSCs *in vitro*.

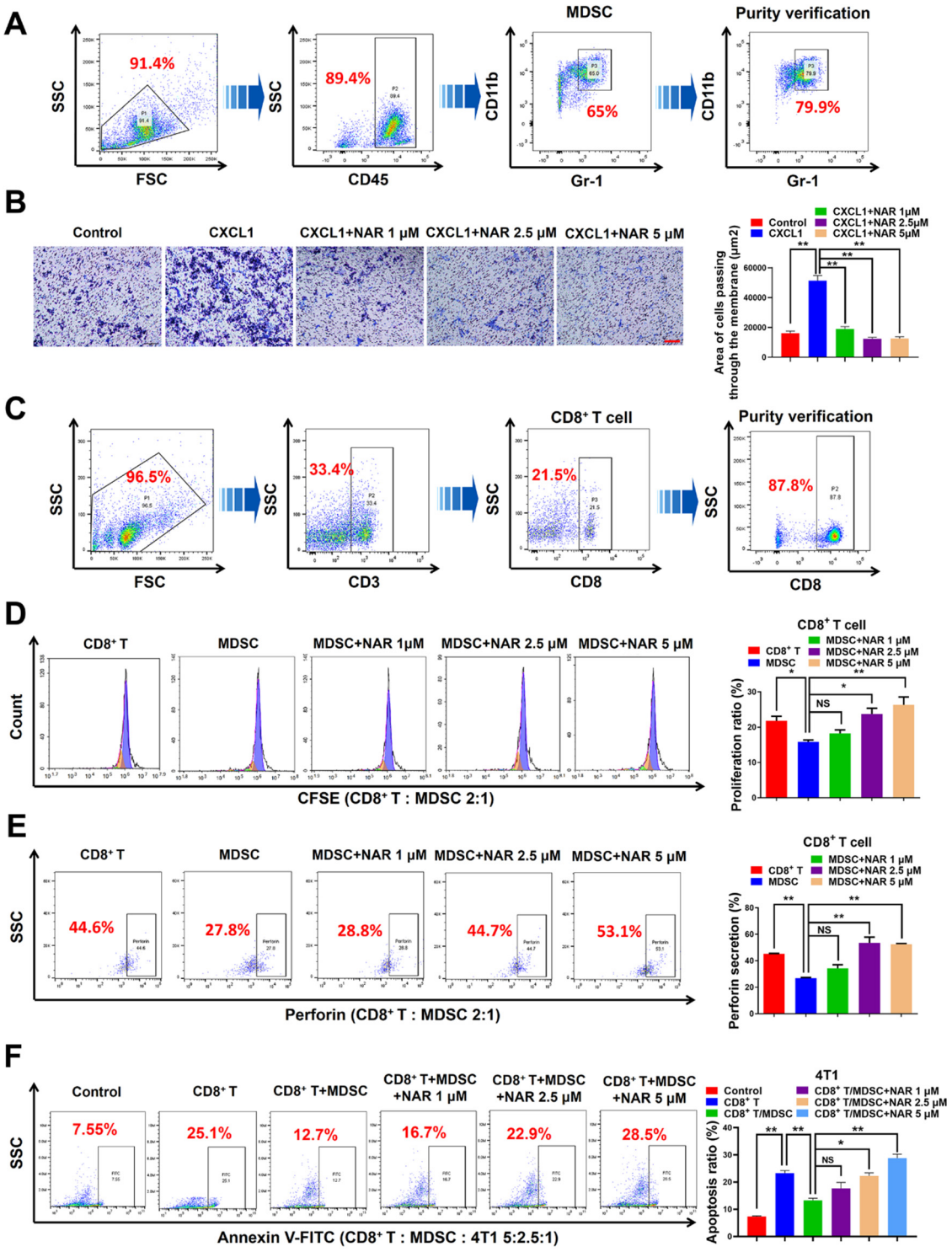

Fig. 5 NAR inhibited MDSC metastasis and reversed its immunosuppressive effects. (A) The sorting strategy of MDSCs by FACS**. (B)** NAR inhibited the metastasis of MDSCs treated with 10 ng/mL CXCL1. Scale bar = 100 μm. Areas of cells passing through the membrane were measured. **(C)** The sorting strategy of $CD8^+$ T cells by FACS**. (D)** CFSE assay results for $CD8^+$ T cell proliferation after co-culture with MDSCs treated with 10 ng/mL CXCL1 or NAR (1–5 μmol/L). The proliferation percentages of $CD8^+$ T cells were measured. **(E)** Detection of perforin secretion of $CD8^+$ T cells in a co-culture system with MDSCs treated with 10 ng/mL CXCL1 or NAR by flow cytometry. **(F)** The cell apoptosis rate of 4T1 cells was detected after co-culture with $CD8^+$ T cells or CXCL1-treated MDSCs in the presence of NAR. Data are presented as mean ± SD, n = 3, $^*P < 0.05$, $^{**}P < 0.01$.

To validate the crucial role of CXCR2 in mediating the pharmacological activities of NAR, we isolated MDSCs from CXCR2-KO mice **(Fig. 6A)**. The results showed that CXCR2-KO significantly blocked the CXCL1-induced invasion ability of MDSCs, and the inhibitory effect of NAR on CXCL1-induced invasion

of MDSCs was also diminished **(Fig. 6B)**. Moreover, in the $CD8^+$ T and MDSC co-culture system, although CXCR2-KO MDSCs still significantly suppressed the proliferation, perforin secretion and apoptosis-induction ability of $CD8^+$ T cells, the stimulatory effects of NAR on $CD8^+$ T activities were reduced following CXCR2-KO (**Fig. 6C–E**). All these results indicate that CXCR2 is a key molecular target of NAR in modulating MDSC activities.

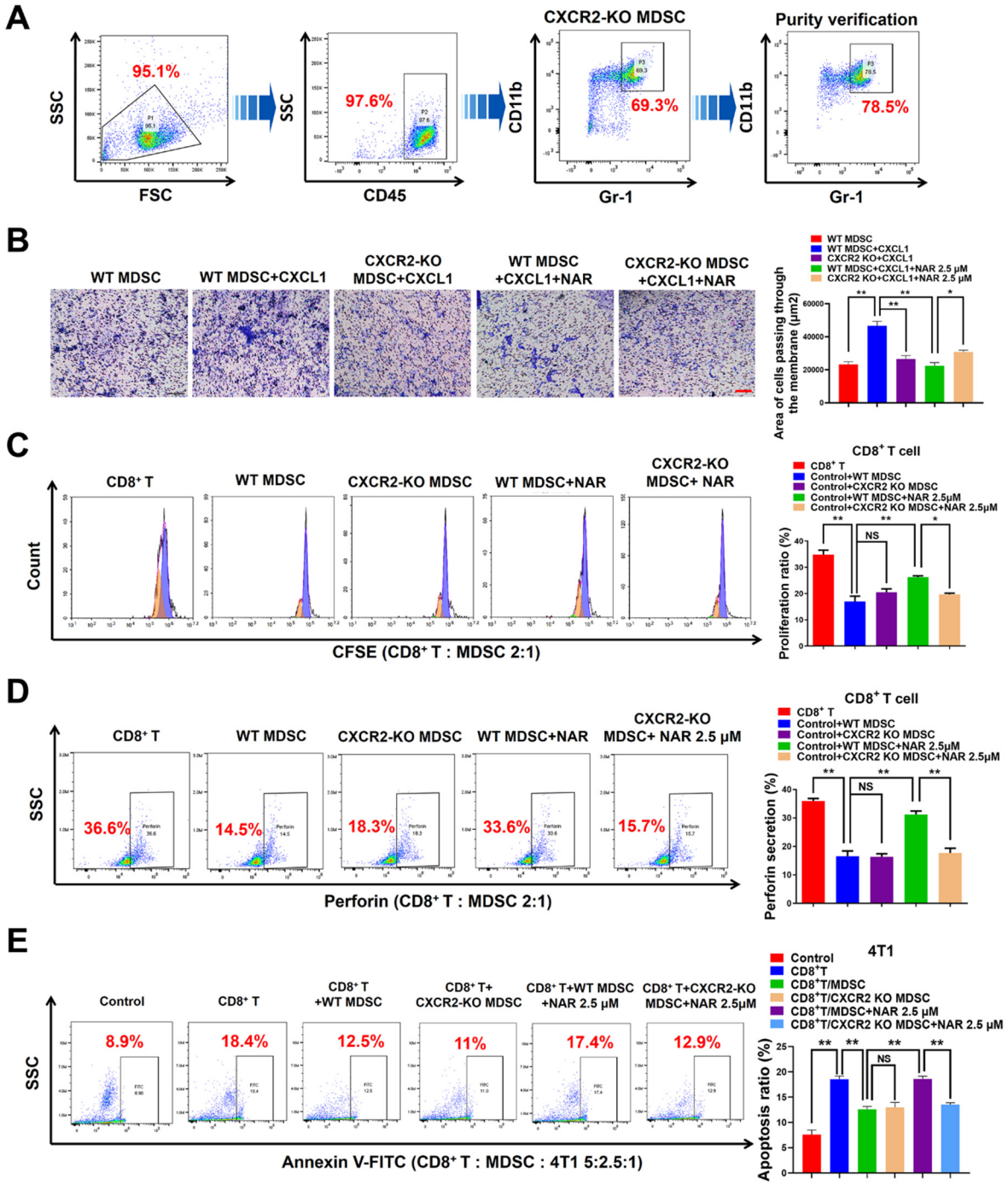

Fig. 6 NAR inhibited MDSC metastasis and reversed its immunosuppressive effects by targeting CXCR2. (A) The sorting strategy of CXCR2-KO MDSCs by FACS**. (B)** Transwell assay for detection of WT or CXCR2-KO MDSC metastasis after treatment with 10 ng/mL CXCL1 or 2.5 μmol/L NAR. Scale bar = 100 μm. Areas of cells passing through the membrane were measured. **(C)** The CFSE assay for $CD8^+$ T cell proliferation after co-culture with WT or CXCR2-KO MDSCs treated with CXCL1 or NAR. The proliferation percentages of $CD8^+$ T cells were measured. **(D)** Detection of perforin secretion of $CD8^+$ T cells co-cultured with WT or CXCR2-KO MDSCs treated with CXCL1 or NAR by flow cytometry. **(E)** 4T1 cell apoptosis rate was detected after co-culture with $CD8^+$ T cells or CXCL1-treated WT/CXCR2-KO MDSCs in the presence of NAR. Data are presented as mean ± SD, n = 3, $^*P < 0.05$, $^{**}P < 0.01$.

3.6 NAR inhibits the recruitment and immunosuppressive activity of MDSCs in the zebrafish xenotransplantation model

To investigate the modulatory effects of NAR on MDSCs *in vivo*, the zebrafish xenotransplant model was employed. Firstly, we evaluated the *in vivo* toxic effect of NAR on zebrafish embryos. As shown in **Fig. S6A–C**, NAR displayed negligible embryotoxicity or teratogenic effect within 48 h and only displayed minimal teratogenic effect beyond 72 h at the highest dosage of 100 μmol/L. Subsequently, CXCL1-treated MDSCs were injected into zebrafish and labeled with Dio. It was observed that CXCL1 promoted MDSC metastasis dose-dependently, which was remarkably inhibited by CXCR2 inhibitor SB225002 (**Fig. 7A**), suggesting that CXCR2 is crucial for MDSC recruitment *in vivo*. To observe the inhibitory effect of NAR on MDSC recruitment and subsequent 4T1 metastasis, we firstly injected CXCL1-treated MDSCs into zebrafish with or without NAR treatment for 12 h, and then injected 4T1 cells and observed their metastasis after 3 h. It was found that NAR dose-dependently inhibited CXCL1-induced MDSC recruitment. More importantly, 4T1 metastasis was also remarkably inhibited, which might be closely correlated with reduced MDSC recruitment towards the caudal vein plexus (**Fig. 7B**). To validate the crucial role of CXCR2 in mediating the pharmacological activities of NAR, the WT or CXCR2-KO MDSCs were pretreated with CXCL1 and subsequently co-injected with 4T1 and $CD8^+$ T cells, and zebrafish were further treated with or without NAR. As shown in **Fig. 7C**, 4T1 fluorescence intensity as well as the number of metastatic foci were significantly diminished after $CD8^+$ T cell co-injection. However, the diminution was reversed after the addition of either WT or CXCR2-KO MDSCs, and the cytotoxic limiting effect of CXCR2-KO MDSCs was weaker compared to WT MDSCs, suggesting that CXCR2-KO might inhibit the immunosuppressive effect of MDSCs. More importantly, NAR treatment dose-dependently recovered the cytotoxic activity of $CD8^+$ T cells, accompanied by the reduced growth and metastasis of 4T1 cells, indicating that NAR effectively limited the immunosuppressive activity of MDSCs. Notably, the suppression effect of NAR disappeared following CXCR2-KO, indicating that NAR exerted its inhibitory effect on MDSCs *via* CXCR2.

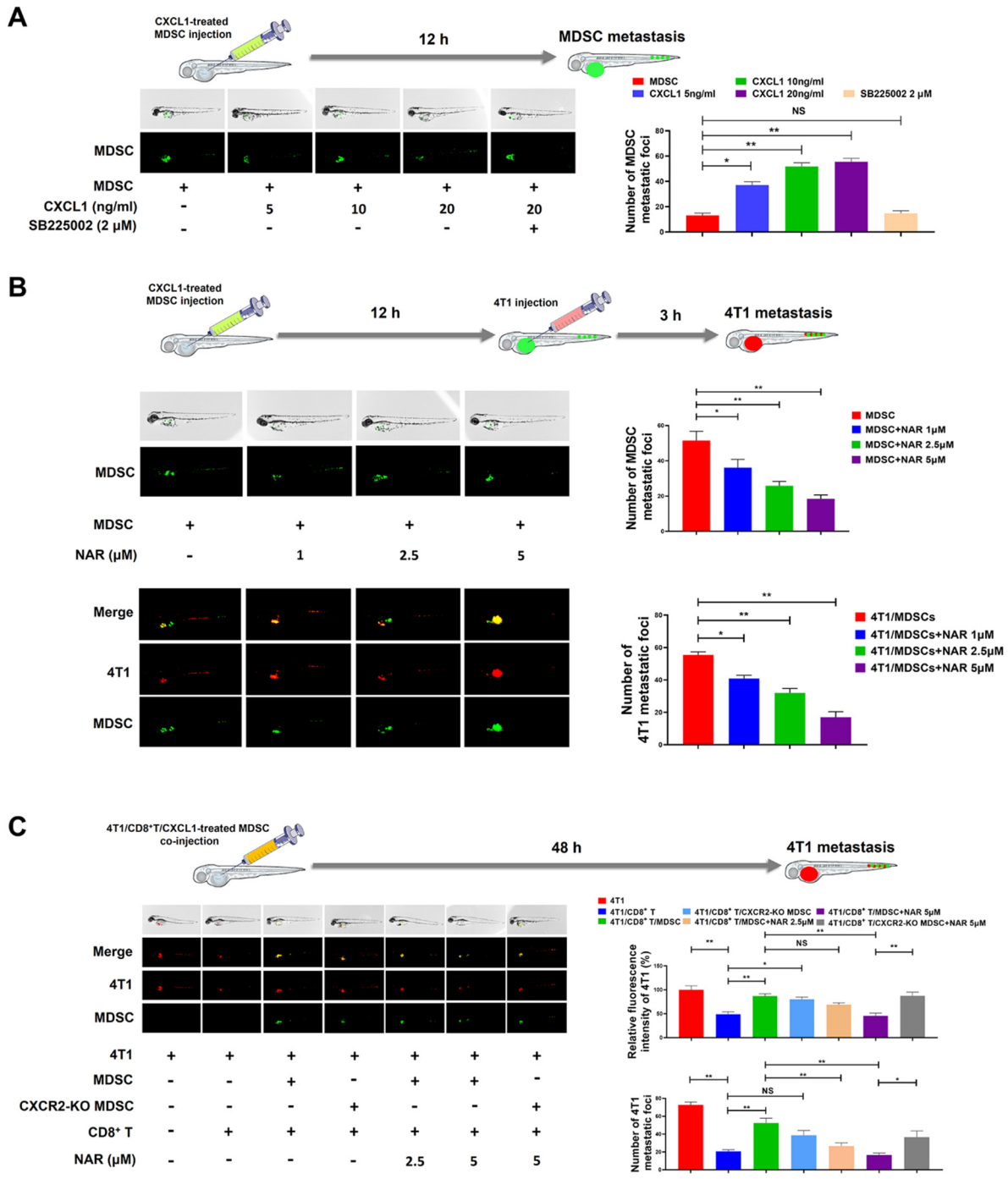

Fig. 7 NAR inhibited MDSC metastasis and subsequent 4T1 metastasis in the zebrafish xenotransplantation model. **(A)** 5–20 ng/mL CXCL1 promoted MDSC metastasis in the zebrafish xenotransplantation model after injection for 12 h, which was reversed by SB225002 treatment. The number of metastatic MDSCs was counted. **(B)** 2.5–5 μmol/L NAR inhibited MDSC metastasis after CXCL1-treated MDSCs were pre-injected for 12 h, and the metastasis of subsequently injected 4T1 cells was also suppressed. The numbers of metastatic MDSCs and 4T1 cells were counted. **(C)** 4T1 cells, $CD8^+$ T cells and CXCL1-treated WT or CXCR2-KO MDSCs were co-injected into zebrafish, and treated with 2.5–5 μmol/L NAR for 48 h. The fluorescence intensities of Dil-stained 4T1 cells were measured. The metastatic number of 4T1 cells was counted. Data are presented as mean ± SD, n = 6, $^*P < 0.05$, $^{**}P < 0.01$.

3.7 NAR inhibits breast cancer PMN formation and lung metastasis by limiting MDSC recruitment and CXCR2 phosphorylation

To further validate the inhibitory effect of NAR on PMN formation *in vivo*, a breast cancer xenograft model was established by injecting 4T1 cells into the mammary glands of Balb/c mice. NAR was administered by intraperitoneal injection daily at dosages of 10 mg/kg/d or 25 mg/kg/d, and the MDSC populations in the

lung, tumor and blood were measured weekly (**Fig. 8A**). The results showed that the lung metastatic lesions were observed in the 4th week in the anatomical specimen of the control group. Concurrently, we noted the presence of regions exhibiting heightened staining intensity, indicative of lung metastatic lesions, within the HE-stained specimens from the control group. However, NAR treatment dose-dependently limited lung metastasis, and minimal metastatic lesions were observed in the 4th week when 25 mg/kg/d NAR was administered, which is similar to those of the CXCR2 inhibitor SB225002 group (**Fig. 8B**). More importantly, we utilized CD11b and Gr-1 staining to observe the distribution of MDSCs in the lung tissues, and CK19 was used to trace the infiltration of 4T1 cells. It was found that as early as the 2nd week, MDSCs were recruited to the lung in the control group, suggesting the formation of PMN. Meanwhile, 4T1 cell infiltration in the lung was found in the 3rd week in the control group following PMN formation. However, NAR treatment and SB225002 administration significantly inhibited MDSC recruitment and 4T1 infiltration in the lung, demonstrating the PMN inhibitory effect of NAR (**Fig. 8C**). Moreover, flow cytometry analysis also revealed that NAR treatment significantly inhibited the MDSC population in the lung, tumor and blood from the 2nd to 4th week. Similar results were also observed in the SB225002 group (**Fig. 8D**). These results demonstrated that NAR inhibited the recruitment of MDSCs *in vivo* and prevented PMN formation.

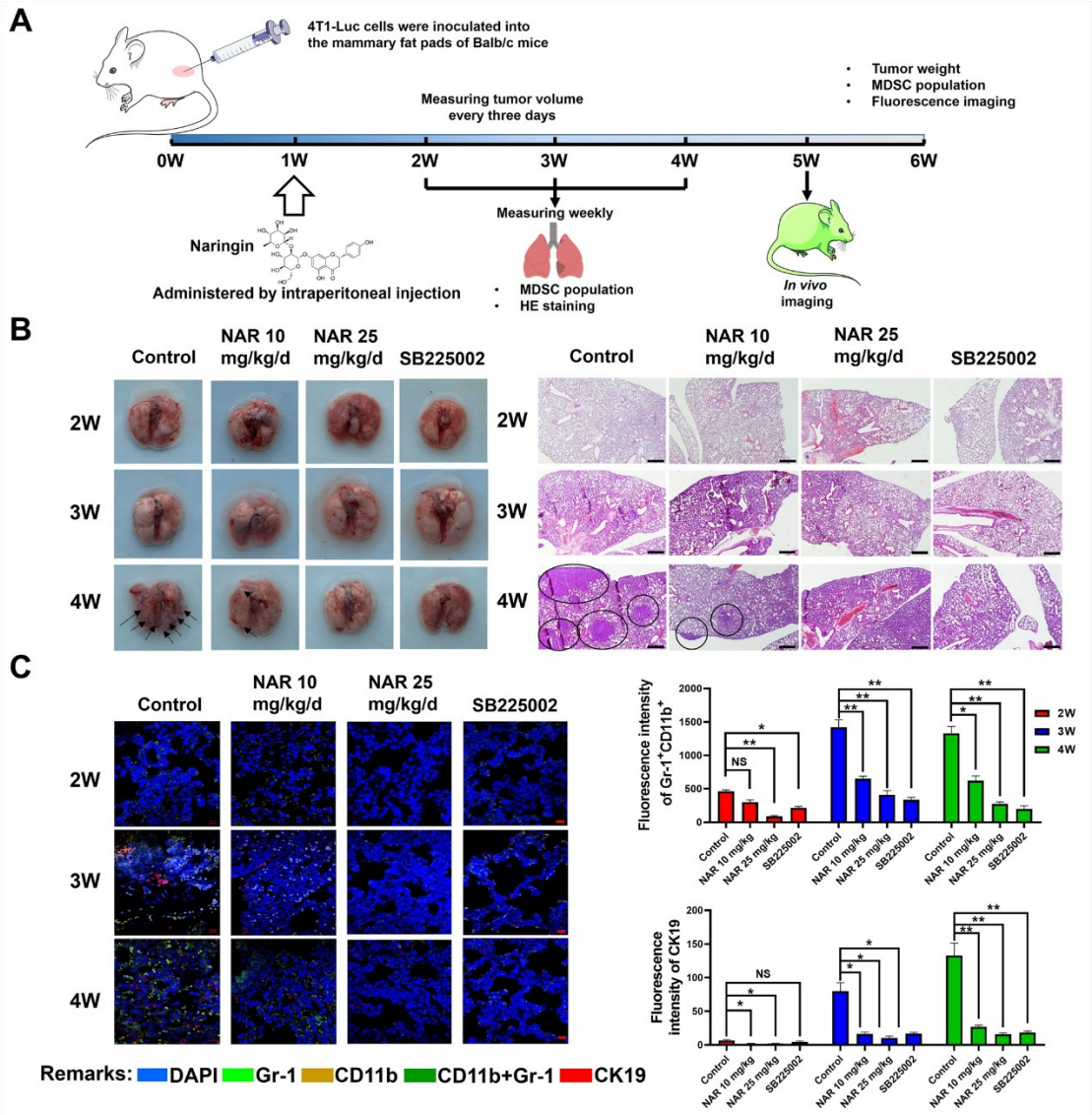

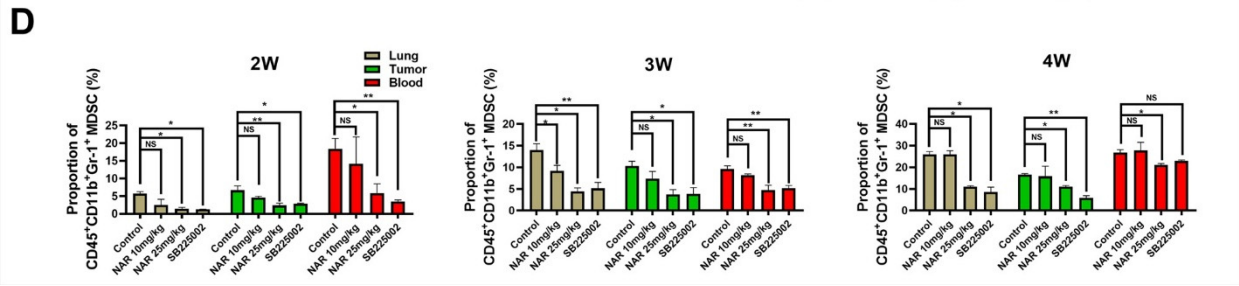

Fig. 8 NAR inhibited PMN formation by suppressing MDSC metastasis *in vivo*. (A) The flowchart of the *in vivo* study. **(B)** Representative images of the harvested lungs and HE staining of lung tissues from mice treated with 10–25 mg/kg/d NAR or 2 mg/kg/d SB225002 for 2, 3 and 4 weeks, respectively. Scale bar = 500 μm. **(C)** Representative immunofluorescence images of lungs from mice treated with NAR or SB225002 for 2, 3 and 4 weeks, respectively. Fluorescence intensities of $CD11b^{+}/Gr\text{-}1^{+}$ and $CK19^{+}$ were measured, respectively. Scale bar = 10 μm. **(D)** MDSC populations in lungs, tumor tissues and peripheral blood samples from mice treated with NAR for 2, 3 and 4 weeks were detected by flow cytometry. Data are presented as mean ± SD, n = 3, $^{*}P < 0.05$, $^{**}P < 0.01$.

At the end of the animal experiment, NAR dose-dependently inhibited breast cancer growth and lung metastasis, and the inhibition ratio was comparable to SB225002 (**Fig. 9A**). Luciferase imaging results also revealed that the metastatic burdens in NAR and SB225002 groups were dramatically inhibited (**Fig. 9B**), accompanied by the reduced number of circulating tumor cells, presenting as decreased Luciferase mRNA levels in the blood (**Fig. 9C**). Meanwhile, flow cytometry analysis further validated that NAR and SB225002 could effectively inhibit the MDSC population in the tumor, blood and lung tissues in the 6th week, which was consistent with the findings from the 2nd to 4th week (**Fig. 9D**). Finally, spleen-derived MDSCs from tumor-bearing mice were acquired through FACS strategies, and immunofluorescence was applied to detect the phosphorylation of CXCR2. As shown in **Fig. 9E**, CXCR2 phosphorylation was significantly suppressed in splenic MDSCs treated with NAR and SB225002, indicating that NAR could effectively target CXCR2 expressed on MDSCs *in vivo*. These results demonstrated that NAR could effectively inhibit MDSC recruitment and block PMN formation *in vivo*, and ultimately suppress the growth and metastasis of breast cancer.

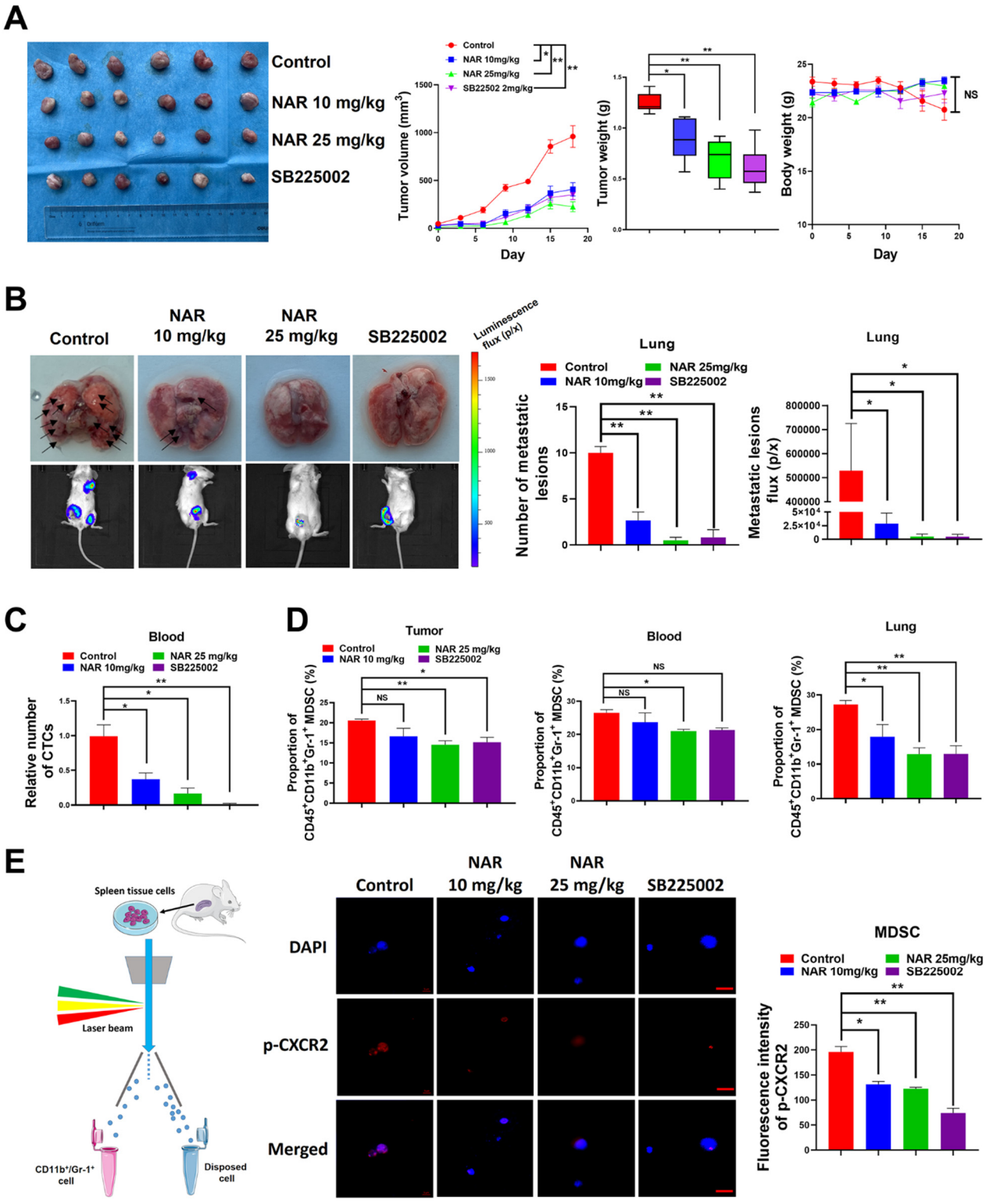

Fig. 9 NAR inhibited breast cancer growth, metastasis and CXCR2 phosphorylation *in vivo*. (A) Representative images of tumors from breast cancer-bearing mice treated with 10–25 mg/kg/d NAR or 2 mg/kg/d SB225002. The tumor growth curve, tumor weight and mouse body weight were measured. n = 6. **(B)** Representative images of the harvested lungs and the *in vivo* imaging assay of tumor-bearing mice treated with NAR or SB225002.The number of lung metastatic lesions was counted and the luminescent intensities were measured. n = 3. **(C)** CTCs in the peripheral blood of mice from various groups were quantified by QPCR. The mRNA transcription levels of the Luciferase gene in peripheral blood samples from tumor-bearing mice were detected. n = 3. **(D)** MDSC populations in tumor tissues, lung tissues and peripheral blood samples from tumor-bearing mice treated with NAR or SB225002 were detected by flow cytometry. n = 6. **(E)** Representative immunofluorescence images of splenic MDSCs stained with p-CXCR2 antibody. Fluorescence intensities of p-CXCR2 were measured. Scale bar = 10 μm. Data are presented as mean ± SD, n = 3, $^{*}P < 0.05$, $^{**}P < 0.01$.

4. Discussion

Targeting CXCR2 to develop novel anti-cancer drugs is a hot topic in oncology research. Current small molecular CXCR2 inhibitors have been shown to regulate the tumor immune microenvironment. CXCR2 antagonists, such as SB225002 and SX-682, could promote B cell and NK cell infiltration and reduce MDSC infiltration in multiple malignancies [12, 51, 52]. However, to date, no CXCR2 inhibitors have been approved for clinical use in anti-cancer treatment. A major challenge in clinical application is that systemic inhibition of CXCR2 leads to compensatory increases in corresponding ligands (such as CXCL2 and CXCL1), resulting in undesirable side effects such as inflammation and affecting therapeutic efficacy [53]. Therefore, identifying CXCR2 inhibitors from natural compounds has become a promising strategy for drug discovery. Herein, NAR was identified as a potential CXCR2 antagonist through computer-aided strategy and BLI assay. NAR was demonstrated to mitigate the immunosuppressive actions of MDSCs and limit their migration, thus obstructing the formation of PMN. In nature, NAR is abundantly detected in the citrus category, such as tomatoes, cherries, and grapefruit. With a flavonoid-like structure, NAR may be effective in preventing the compensatory inflammatory responses typically induced by CXCR2 inhibition. For instance, it was found that NAR could alleviate LPS-induced airway inflammation, a primary adverse reaction associated with CXCR2 inhibition [54, 55]. Meanwhile, NAR demonstrated excellent safety profiles in multiple *in vivo* toxicity studies [56]. Therefore, NAR might overcome the limitations of current CXCR2 inhibitors, and holds considerable promise for clinical applications with high safety.

Computer-aided virtual screening strategies provide a highway for the discovery of small molecules. Although several high-resolution 3D crystal structures of the CXCR2 protein have been determined in recent years [57, 58], these structures remain largely incomplete. Therefore, we employed a ligand-based pharmacophore screening approach. Pharmacophore modeling was firstly applied in computer-aided drug design in 1991[59]. By analyzing the common features of known ligands, the detailed structural information of the receptors is not required in pharmacophore modeling [60]. As a sophisticated strategy in virtual screening, pharmacophore modeling has been applied in anti-cancer drug discovery in recent years, such as in the development of avapritinib derivatives for gastrointestinal stromal cancer and novel STAT3 antagonists for non-small cell lung cancer [61, 62]. In this study, two distinct CXCR2 pharmacophore models were established to screen a total of 15,000 natural compounds. Following validation by the BLI assay, four compounds including 9'''-methyl lithospermate B, thiostrepton, rhoifolin, and NAR were identified as CXCR2 potential inhibitors. Among the four candidates, although thiostrepton had the highest binding affinity, NAR showed the strongest inhibition activity on CXCR2 phosphorylation and the activation of downstream STAT3 signaling. Meanwhile, the DARTS assay further demonstrated that CXCR2 was the protein target of NAR. All these findings suggest that NAR is a natural CXCR2 inhibitor. Although increasing studies have revealed that NAR could inhibit the progression of multiple malignancies by modulation of oxidative stress, autophagy, aerobic glycolysis and gut microbiota [63-66], our study firstly identified CXCR2 as the direct target of NAR. Moreover, through the integration of multiple techniques

including pharmacophore modeling analysis, BLI assay, DARTS validation, and molecular function experiments, our study provided a comprehensive approach to drug discovery.

MDSCs are crucial immunosuppressive cells in the tumor microenvironment. MDSCs mainly originate from bone marrow, and can be classified into monocytic MDSC (mMDSC) or granulocytic MDSC (gMDSC) [8]. High levels of MDSC infiltration were observed in late-stage cancer patients, and MDSC levels were also positively correlated with the metastatic burden of breast cancer patients [67, 68]. Therefore, MDSCs are considered an essential target for breast cancer immunotherapy [69]. Current strategies for inhibiting MDSCs include reducing their generation, inactivating their recruitment, and promoting their differentiation [70, 71]. Among these approaches, targeting CXCR2 to prevent its recruitment has garnered extensive attention. For example, it has been found that targeting CXCR2 on MDSCs could significantly promote NK cell cytotoxicity, trigger anti-tumor immunity and suppress metastasis in multiple malignancies [72]. Particularly, the interaction between the CXCR2 and its ligands, such as CXCL1, plays a crucial role in MDSC recruitment and infiltration in tumors. In addition, the CXCL1/CXCR2 axis was able to sustain the survival and suppressive immunomodulatory abilities of MDSCs in TME [73]. Our previous study found that CXCL1/CXCR2 signaling induced the migration of spleen-derived MDSCs to the lungs, promoting the formation of PMN in a breast cancer mouse model [73, 74]. In this study, it was found that NAR effectively inhibited MDSC recruitment by interrupting the interaction between CXCL1 and CXCR2. NAR decreased MDSC migration and their ability to recruit tumor cells. Meanwhile, the suppressive activity of MDSCs on $CD8^+$ T cells was also inhibited by NAR both *in vitro* and in the zebrafish breast cancer model. Considering the low toxicity of NAR, it is promising to develop NAR-based strategies to inhibit MDSCs by targeting CXCR2.

PMN provides a microenvironment that is congenial for cancer cell invasion, seeding, endurance, and proliferation. The primary therapeutic strategies for inhibiting PMN formation focus on neutralizing antibodies against tumor-secreted cytokines, such as VEGF and lysyl oxidase (LOX), as well as specific antagonists targeting immunosuppressive cells, such as CCR2 and CXCR2 inhibitors. However, most of these candidate drugs are still in the clinical trial stage, with no specific PMN antagonists available currently [75]. A significant challenge is the problem of off-target and specific side effects. Interestingly, emerging studies have highlighted the potential of natural compounds such as curcumin and icaritin in suppressing MDSC recruitment and ameliorating PMN formation [76], with some of these compounds also undergoing clinical trials. It has been reported that icaritin can enhance the immune response of the anti-PD-1 strategy and increase survival in advanced-stage hepatocellular carcinoma patients [77]. Although natural compounds generally tend to have milder potency on specific targets compared to neutralizing antibodies or synthetic small-molecule inhibitors, they offer better comprehensive effects with fewer adverse reactions [78]. However, currently, there is a lack of high-throughput screening studies for identifying natural inhibitors targeting PMN. Herein, we identified NAR as a promising therapeutic agent for inhibiting PMN formation through *in silico* virtual screening combined with molecular validation assays. As early as two weeks

following NAR treatment, the population of MDSCs in the lung PMN decreased. Meanwhile, CXCR2 phosphorylation of spleen-derived MDSCs was also suppressed by NAR. Since the spleen is the main origin of MDSCs, this phenomenon suggests that NAR might inhibit MDSC recruitment towards PMN by targeting CXCR2. Furthermore, we also found that NAR significantly inhibited breast cancer lung metastasis and CTCs, which was closely correlated with the suppressed PMN formation. However, the therapeutic value of NAR in inhibiting PMN formation still requires structural modifications, targeting optimization, and clinical trial validation in the future.

Taken together, our results identify NAR as a natural CXCR2 antagonist, and shed novel light on its role in inhibiting PMN formation in breast cancer by suppressing MDSC recruitment. Our findings not only highlight the value of CXCR2 as a significant therapeutic target for preventing PMN formation, but also present NAR as a promising natural compound for improving TNBC prognosis. Further investigation is anticipated to develop NAR-based strategies to improve therapeutic efficacy and prognosis in breast cancer.

5. Conclusion

In summary, our research integrated virtual screening and *in vitro* validation strategies to identify NAR as a potential CXCR2 inhibitor, and revealed that NAR could inhibit PMN formation and breast cancer progression *by* inhibiting the mobilization of MDSCs through targeting CXCR2. Our study not only discovered NAR as a potential CXCR2 antagonist, but also revealed the novel pharmacological activity of NAR in inhibiting PMN formation.

Acknowledgements

This work was supported by the National Natural Science Foundation of China [82374446]; the State Key Laboratory of Dampness Syndrome of Chinese Medicine [SZ2021ZZ19]; the Science and Technology Planning Project of Guangdong Province [2022B1515230002, 2023B1212060063]; the 2020 Guangdong Provincial Science and Technology Innovation Strategy Special Fund (Guangdong-Hong Kong-Macau Joint Lab) [2020B1212030006]; the Guangzhou Basic and Applied Basic Research Foundation [2023A03J0223, 2025A03J4135, 2025CX009]; the Specific Research Fund for TCM Science and Technology of Guangdong provincial Hospital of Chinese Medicine [YN2023MS31], and the Open Research Fund of Chengdu University of Traditional Chinese Medicine State Key Laboratory Southwestern Chinese Medicine Resources.

Competing interests

No potential competing interests are disclosed by the authors.

Supplementary information

Supplementary information is available at the website of Food Science and Human Wellness.

Declaration of AI and AI-assisted Technologies

No AI or AI-assisted technologies were used.

Reference

[1] F. Bray, M. Laversanne, H.Y.A. Sung, et al., Global cancer statistics 2022: GLOBOCAN estimates of incidence and mortality worldwide for 36 cancers in 185 countries, Ca-Cancer J Clin. 74 (2024) 229-263. https://doi.org/10.3322/caac.21834.

[2] B. Gerber, E. Seitz, H. Muller, et al., Perioperative screening for metastatic disease is not indicated in patients with primary breast cancer and no clinical signs of tumor spread, Breast Cancer Res Treat. 82 (2003) 29-37. https://doi.org/10.1023/B:BREA.0000003917.05413.ac.

[3] N. Harbeck, M. Gnant, Breast cancer, Lancet. 389 (2017) 1134-1150. https://doi.org/10.1016/S0140-6736(16)31891-8.

[4] R.N. Kaplan, R.D. Riba, S. Zacharoulis, et al., VEGFR1-positive haematopoietic bone marrow progenitors initiate the pre-metastatic niche, Nature. 438 (2005) 820-827. https://doi.org/10.1038/nature04186.

[5] H. Peinado, H. Zhang, I.R. Matei, et al., Pre-metastatic niches: organ-specific homes for metastases, Nat Rev Cancer. 17 (2017) 302-317. https://doi.org/10.1038/nrc.2017.6.

[6] C. Lai, S. August, R. Behar, et al., Characteristics of immunosuppressive regulatory T cells in cutaneous squamous cell carcinomas and role in metastasis, Lancet. 385 Suppl 1 (2015) S59. https://doi.org/10.1016/S0140-6736(15)60374-9.

[7] K. Nakamura, M.J. Smyth, Myeloid immunosuppression and immune checkpoints in the tumor microenvironment, Cell Mol Immunol. 17 (2020) 1-12. https://doi.org/10.1038/s41423-019-0306-1.

[8] A.M.K. Law, F. Valdes-Mora, D. Gallego-Ortega, Myeloid-Derived Suppressor Cells as a Therapeutic Target for Cancer, Cells-Basel. 9 (2020) https://doi.org/ARTN 56110.3390/cells9030561.

[9] T. Condamine, I. Ramachandran, J.I. Youn, et al., Regulation of tumor metastasis by myeloid-derived suppressor cells, Annu Rev Med. 66 (2015) 97-110. https://doi.org/10.1146/annurev-med-051013-052304.

[10] Y. Wang, Y. Ding, N. Guo, et al., MDSCs: Key Criminals of Tumor Pre-metastatic Niche Formation, Front Immunol. 10 (2019) 172. https://doi.org/10.3389/fimmu.2019.00172.

[11] A. Stadtmann, A. Zarbock, CXCR2: From Bench to Bedside, Front Immunol. 3 (2012) 263. https://doi.org/10.3389/fimmu.2012.00263.

[12] S. Greene, Y. Robbins, W.K. Mydlarz, et al., Inhibition of MDSC Trafficking with SX-682, a CXCR1/2 Inhibitor, Enhances NK-Cell Immunotherapy in Head and Neck Cancer Models, Clin Cancer Res. 26 (2020) 1420-1431. https://doi.org/10.1158/1078-0432.CCR-19-2625.

[13] B. Jing, T. Wang, B. Sun, et al., IL6/STAT3 Signaling Orchestrates Premetastatic Niche Formation and Immunosuppressive Traits in Lung, Cancer Res. 80 (2020) 784-797. https://doi.org/10.1158/0008-5472.CAN-19-2013.

[14] Y. Cheng, F. Mo, Q. Li, et al., Targeting CXCR2 inhibits the progression of lung cancer and promotes therapeutic effect of cisplatin, Mol Cancer. 20 (2021) 62. https://doi.org/10.1186/s12943-021-01355-1.

[15] S. Cabrero-de Las Heras, E. Martinez-Balibrea, CXC family of chemokines as prognostic or predictive biomarkers and possible drug targets in colorectal cancer, World J Gastroenterol. 24 (2018) 4738-4749. https://doi.org/10.3748/wjg.v24.i42.4738.

[16] M. Taki, K. Abiko, T. Baba, et al., Snail promotes ovarian cancer progression by recruiting myeloid-derived suppressor cells via CXCR2 ligand upregulation, Nat Commun. 9 (2018) 1685. https://doi.org/10.1038/s41467-018-03966-7.

[17] S. Kumar, D.W. Wilkes, N. Samuel, et al., DeltaNp63-driven recruitment of myeloid-derived suppressor cells promotes metastasis in triple-negative breast cancer, J Clin Invest. 128 (2018) 5095-5109. https://doi.org/10.1172/JCI99673.

[18] T.E. Keenan, S.M. Tolaney, Role of Immunotherapy in Triple-Negative Breast Cancer, J Natl Compr Canc Netw. 18 (2020) 479-489. https://doi.org/10.6004/jnccn.2020.7554.

[19] J.R. White, J.M. Lee, P.R. Young, et al., Identification of a potent, selective non-peptide CXCR2 antagonist that inhibits interleukin-8-induced neutrophil migration, J Biol Chem. 273 (1998) 10095-10098. https://doi.org/10.1074/jbc.273.17.10095.

[20] M.P. Dwyer, Y. Yu, CXCR2 modulators: a patent review (2009 - 2013), Expert Opin Ther Pat. 24 (2014) 519-534. https://doi.org/10.1517/13543776.2014.887682.

[21] L.J. Goldstein, R.P. Perez, D. Yardley, et al., Correction to: A window-of-opportunity trial of the CXCR1/2 inhibitor reparixin in operable HER-2-negative breast cancer, Breast Cancer Res. 22 (2020) 52. https://doi.org/10.1186/s13058-020-01294-7.

[22] O. Holz, S. Khalilieh, A. Ludwig-Sengpiel, et al., SCH527123, a novel CXCR2 antagonist, inhibits ozone-induced neutrophilia in healthy subjects, Eur Respir J. 35 (2010) 564-570. https://doi.org/10.1183/09031936.00048509.

[23] R.B. Moss, S.J. Mistry, M.W. Konstan, et al., Safety and early treatment effects of the CXCR2 antagonist SB-656933 in patients with cystic fibrosis, J Cyst Fibros. 12 (2013) 241-248. https://doi.org/10.1016/j.jcf.2012.08.016.

[24] J.-T. Li, A. Gu, N.-N. Tang, et al., Exploring anti-tumor potential of food and medicine homology substances: An in-silico evaluation of Citri Grandis Exocarpium against gallbladder cancer, Food & Medicine Homology. (2025) https://doi.org/10.26599/FMH.2026.9420084.

[25] M.-Y. Li, Q. Zhang, J. Li, et al., Food and medicine homology in cancer treatment: traditional thoughts collide with scientific evidence, Food & Medicine Homology. 2 (2025) 9420120. https://doi.org/10.26599/FMH.2025.9420120.

[26] B. Gentile, J. Mehrez, T. Milosavljevic, et al., An angiogenic proteome study of black raspberry extract on neuroendocrine cancers, Clinical Traditional Medicine and Pharmacology. 6 (2025) https://doi.org/10.1016/j.ctmp.2025.200198.

[27] G.K. Shikha Sharma, Nitin Kumar, Neeraj K. Sethiya, Dheeraj Bisht, Diuretic Activity of Ethanol Extract of Piper attenuatum Leaves Might Be Due to the Inhibition of Carbonic Anhydrase Enzyme: An in vivo and in silico Investigation, Clinical Complementary Medicine and Pharmacology. 4 (2024), https://doi.org/10.1016/j.ccmp.2023.100117

[28] J. Yuan, J. Yu, Y. Huang, et al., Antibiotic fidaxomicin is an RdRp inhibitor as a potential new therapeutic agent against Zika virus, BMC Med. 18 (2020) 204. https://doi.org/10.1186/s12916-020-01663-1.

[29] S. Gangadevi, V.N. Badavath, A. Thakur, et al., Kobophenol A Inhibits Binding of Host ACE2 Receptor with Spike RBD Domain of SARS-CoV-2, a Lead Compound for Blocking COVID-19, J Phys Chem Lett. 12 (2021) 1793-1802. https://doi.org/10.1021/acs.jpclett.0c03119.

[30] S. Wang, N. Wang, X. Huang, et al., Baohuoside i suppresses breast cancer metastasis by downregulating the tumor-associated macrophages/C-X-C motif chemokine ligand 1 pathway, Phytomedicine. 78 (2020) 153331. https://doi.org/10.1016/j.phymed.2020.153331.

[31] M.P. Dwyer, Y. Yu, J. Chao, et al., Discovery of 2-hydroxy-N,N-dimethyl-3-2-[[(R)-1-(5-methylfuran-2-yl)propyl]amino]-3,4-dioxocyclobut-1-enylaminobenzamide (SCH 527123): a potent, orally bioavailable CXCR2/CXCR1 receptor antagonist, J Med Chem. 49 (2006) 7603-7606. https://doi.org/10.1021/jm0609622.

[32] Q. Jin, H. Nie, B.W. McCleland, et al., Discovery of potent and orally bioavailable N,N'-diarylurea antagonists for the CXCR2 chemokine receptor, Bioorg Med Chem Lett. 14 (2004) 4375-4378. https://doi.org/10.1016/j.bmcl.2004.06.097.

[33] B.W. McCleland, R.S. Davis, M.R. Palovich, et al., Comparison of N,N'-diarylsquaramides and N,N'-diarylureas as antagonists of the CXCR2 chemokine receptor, Bioorg Med Chem Lett. 17 (2007) 1713-1717. https://doi.org/10.1016/j.bmcl.2006.12.067.

[34] J.R. Merritt, L.L. Rokosz, K.H. Nelson, Jr., et al., Synthesis and structure-activity relationships of 3,4-diaminocyclobut-3-ene-1,2-dione CXCR2 antagonists, Bioorg Med Chem Lett. 16 (2006) 4107-4110. https://doi.org/10.1016/j.bmcl.2006.04.082.

[35] H. Nie, K.L. Widdowson, M.R. Palovich, et al., N,N'-Diarylcyanoguanidines as antagonists of the CXCR2 and CXCR1 chemokine receptors, Bioorg Med Chem Lett. 16 (2006) 5513-5516. https://doi.org/10.1016/j.bmcl.2006.08.042.

[36] M.P. Dwyer, Y. Yu, CXCR2 receptor antagonists: a medicinal chemistry perspective, Curr Top Med Chem. 14 (2014) 1590-1605. https://doi.org/10.2174/1568026614666140827144615.

[37] H. Ha, B. Debnath, S. Odde, et al., Discovery of Novel CXCR2 Inhibitors Using Ligand-Based Pharmacophore Models, J Chem Inf Model. 55 (2015) 1720-1738. https://doi.org/10.1021/acs.jcim.5b00181.

[38] J. Che, Z. Wang, H. Sheng, et al., Ligand-based pharmacophore model for the discovery of novel CXCR2 antagonists as anti-cancer metastatic agents, R Soc Open Sci. 5 (2018) 180176. https://doi.org/10.1098/rsos.180176.

[39] B. Lomenick, R. Hao, N. Jonai, et al., Target identification using drug affinity responsive target stability (DARTS), Proc Natl Acad Sci U S A. 106 (2009) 21984-21989. https://doi.org/10.1073/pnas.0910040106.

[40] N. Bai, Y. Guo, M. Zhou, et al., Rhodiola rosea L. improves the immunosuppressive microenvironment through the HIF-1α/TGF-β/Smad signaling pathway in breast cancer, Clinical Traditional Medicine and Pharmacology. 6 (2025) https://doi.org/10.1016/j.ctmp.2024.200185.

[41] S.Q. Wang, N. Wang, X.W. Huang, et al., Baohuoside i suppresses breast cancer metastasis by downregulating the tumor-associated macrophages/C-X-C motif chemokine ligand 1 pathway, Phytomedicine. 78 (2020) https://doi.org/ARTN 15333110.1016/j.phymed.2020.153331.

[42] N. Bai, Q. Wang, C. Zhang, et al., Triterpenoid saponin from Ardisia gigantifolia Stapf inhibits cancer cell metastasis behavior of TNBC via suppressing EMT and stemness through ITGB4/FAK signals, Clinical Traditional Medicine and Pharmacology. 5 (2024) https://doi.org/10.1016/j.ctmp.2024.200182.

[43] Y. Zheng, N. Wang, S. Wang, et al., XIAOPI formula inhibits the pre-metastatic niche formation in breast cancer via suppressing TAMs/CXCL1 signaling, Cell Commun Signal. 18 (2020) 48. https://doi.org/10.1186/s12964-020-0520-6.

[44] W.M. Taylor, C.F. Simpson, F.G. Martin, Certain aspects of toxicity of an amicarbalide formulation to ponies, Am J Vet Res. 33 (1972) 533-541. https://www.ncbi.nlm.nih.gov/pubmed/5014461

[45] X. Shen, L. Wang, C. Xu, et al., Fusion of thymosin alpha 1 with mutant IgG1 CH3 prolongs half-life and enhances antitumor effects in vivo, Int Immunopharmacol. 74 (2019) 105662. https://doi.org/10.1016/j.intimp.2019.05.047.

[46] G. Meissner, Ryanodine activation and inhibition of the Ca2+ release channel of sarcoplasmic reticulum, J Biol Chem. 261 (1986) 6300-6306. https://www.ncbi.nlm.nih.gov/pubmed/2422165

[47] I.U. Schraufstatter, M. Burger, R.C. Hoch, et al., Importance of the carboxy-terminus of the CXCR2 for signal transduction, Biochem Biophys Res Commun. 244 (1998) 243-248. https://doi.org/10.1006/bbrc.1998.8246.

[48] M. Anselmi, F. Fontana, M. Marzagalli, et al., Melanoma Stem Cells Educate Neutrophils to Support Cancer Progression, Cancers (Basel). 14 (2022) https://doi.org/10.3390/cancers14143391.

[49] Y.H. Wang, J.C. Jia, F.Q. Wang, et al., Pre-metastatic niche: formation, characteristics and therapeutic implication, Signal Transduct Tar. 9 (2024) https://doi.org/ARTN 23610.1038/s41392-024-01937-7.

[50] Q. He, W. Huang, D. Liu, et al., Homeobox B5 promotes metastasis and poor prognosis in Hepatocellular Carcinoma, via FGFR4 and CXCL1 upregulation, Theranostics. 11 (2021) 5759-5777. https://doi.org/10.7150/thno.57659.

[51] S. Wang, J. Bai, Y.L. Zhang, et al., CXCL1-CXCR2 signalling mediates hypertensive retinopathy by inducing macrophage infiltration, Redox Biol. 56 (2022) 102438. https://doi.org/10.1016/j.redox.2022.102438.

[52] J.M. Yang, C. Yan, A.E. Vilgelm, et al., Targeted Deletion of CXCR2 in Myeloid Cells Alters the Tumor Immune Environment to Improve Antitumor Immunity, Cancer Immunol Res. 9 (2021) 200-213. https://doi.org/10.1158/2326-6066.Cir-20-0312.

[53] K. Bullock, A. Richmond, Suppressing MDSC Recruitment to the Tumor Microenvironment by Antagonizing CXCR2 to Enhance the Efficacy of Immunotherapy, Cancers (Basel). 13 (2021) https://doi.org/10.3390/cancers13246293.

[54] M. Jain, H.S. Parmar, Evaluation of antioxidative and anti-inflammatory potential of hesperidin and naringin on the rat air pouch model of inflammation, Inflamm Res. 60 (2011) 483-491. https://doi.org/10.1007/s00011-010-0295-0.

[55] H.H. Zhang, X.J. Zhou, Y.S. Zhong, et al., Naringin suppressed airway inflammation and ameliorated pulmonary endothelial hyperpermeability by upregulating Aquaporinl in lipopolysaccharide/cigarette smoke-induced mice, Biomed Pharmacother. 150 (2022) https://doi.org/ARTN 11303510.1016/j.biopha.2022.113035.

[56] P.B. Li, H. Wu, Y.G. Wang, et al., Toxicological evaluation of naringin: Acute, subchronic, and chronic toxicity in Beagle dogs, Regul Toxicol Pharm. 111 (2020) https://doi.org/ARTN 10458010.1016/j.yrtph.2020.104580.

[57] N. Spellmon, J. Holcomb, A. Niu, et al., Structural basis of PDZ-mediated chemokine receptor CXCR2 scaffolding by guanine nucleotide exchange factor PDZ-RhoGEF, Biochem Bioph Res Co. 485 (2017) 529-534. https://doi.org/10.1016/j.bbrc.2017.02.010.

[58] X.J. Shi, Y. Wan, N. Wang, et al., Selection of a picomolar antibody that targets CXCR2-mediated neutrophil activation and alleviates EAE symptoms, Nat Commun. 12 (2021) https://doi.org/ARTN 254710.1038/s41467-021-22810-z.

[59] H. Sun, Pharmacophore-based virtual screening, Curr Med Chem. 15 (2008) 1018-1024. https://doi.org/10.2174/092986708784049630.

[60] C. McInnes, Virtual screening strategies in drug discovery, Curr Opin Chem Biol. 11 (2007) 494-502. https://doi.org/10.1016/j.cbpa.2007.08.033.

[61] A. Teuber, T. Schulz, B.S. Fletcher, et al., Avapritinib-based SAR studies unveil a binding pocket in KIT and PDGFRA, Nat Commun. 15 (2024) https://doi.org/ARTN 6310.1038/s41467-023-44376-8.

[62] Q.Y. Zheng, H. Dong, J.S. Mo, et al., A novel STAT3 inhibitor W2014-S regresses human non-small cell lung cancer xenografts and sensitizes EGFR-TKI acquired resistance, Theranostics. 11 (2021) 824-840. https://doi.org/10.7150/thno.49600.

[63] E.E. Mohamed, O.M. Ahmed, K.M.A. Zoheir, et al., Naringin-Dextrin Nanocomposite Abates Diethylnitrosamine/Acetylaminofluorene-Induced Lung Carcinogenesis by Modulating Oxidative Stress, Inflammation, Apoptosis, and Cell Proliferation, Cancers. 15 (2023) https://doi.org/ARTN 510210.3390/cancers15205102.

[64] S. Raha, S.M. Kim, H.J. Lee, et al., Naringin Induces Lysosomal Permeabilization and Autophagy Cell Death in AGS Gastric Cancer Cells, Am J Chinese Med. 48 (2020) 679-702. https://doi.org/10.1142/S0192415x20500342.

[65] G.T. Pan, P. Zhang, A.Y. Chen, et al., Aerobic glycolysis in colon cancer is repressed by naringin via the pathway, J Zhejiang Univ-Sc B. 24 (2023) 221-231. https://doi.org/10.1631/jzus.B2200221.

[66] B.Q. Xie, X.N. Zhou, C.L. Luo, et al., Reversal of Platinum-based Chemotherapy Resistance in Ovarian Cancer by Naringin Through Modulation of The Gut Microbiota in a Humanized Nude Mouse Model, J Cancer. 15 (2024) 4430-4447. https://doi.org/10.7150/jca.96448.

[67] C.M. Diaz-Montero, M.L. Salem, M.I. Nishimura, et al., Increased circulating myeloid-derived suppressor cells correlate with clinical cancer stage, metastatic tumor burden, and doxorubicin-cyclophosphamide chemotherapy, Cancer Immunol Immun. 58 (2009) 49-59. https://doi.org/10.1007/s00262-008-0523-4.

[68] N. Mirza, M. Fishman, I. Fricke, et al., --retinoic acid improves differentiation of myeloid cells and immune response in cancer patients, Cancer Res. 66 (2006) 9299-9307. https://doi.org/10.1158/0008-5472.Can-06-1690.

[69] E. Safarzadeh, S. Hashemzadeh, P.H.G. Duijf, et al., Circulating myeloid-derived suppressor cells: An independent prognostic factor in patients with breast cancer, J Cell Physiol. 234 (2019) 3515-3525. https://doi.org/10.1002/jcp.26896.

[70] C. Blattner, V. Fleming, R. Weber, et al., CCR5(+) Myeloid-Derived Suppressor Cells Are Enriched and Activated in Melanoma Lesions, Cancer Res. 78 (2018) 157-167. https://doi.org/10.1158/0008-5472.CAN-17-0348.

[71] A. Orillion, A. Hashimoto, N. Damayanti, et al., Entinostat Neutralizes Myeloid-Derived Suppressor Cells and Enhances the Antitumor Effect of PD-1 Inhibition in Murine Models of Lung and Renal Cell Carcinoma, Clin Cancer Res. 23 (2017) 5187-5201. https://doi.org/10.1158/1078-0432.CCR-17-0741.

[72] A. Banuelos, A.L.S. Zhang, H. Berouti, et al., CXCR2 inhibition in G-MDSCs enhances CD47 blockade for melanoma tumor cell clearance, P Natl Acad Sci USA. 121 (2024) https://doi.org/ARTN e231853412110.1073/pnas.2318534121.

[73] H. Katoh, D. Wang, T. Daikoku, et al., CXCR2-expressing myeloid-derived suppressor cells are essential to promote colitis-associated tumorigenesis, Cancer Cell. 24 (2013) 631-644. https://doi.org/10.1016/j.ccr.2013.10.009.

[74] D. Wang, H. Sun, J. Wei, et al., CXCL1 Is Critical for Premetastatic Niche Formation and Metastasis in Colorectal Cancer, Cancer Res. 77 (2017) 3655-3665. https://doi.org/10.1158/0008-5472.CAN-16-3199.

[75] Y. Zhou, M. Han, J. Gao, Prognosis and targeting of pre-metastatic niche, J Control Release. 325 (2020) 223-234. https://doi.org/10.1016/j.jconrel.2020.06.037.

[76] S. Tu, D. Mao, M. Shi, et al., Icaritin ameliorates extracellular microparticles-induced inflammatory pre-metastatic niche via modulating the cGAS-STING signaling, Phytother Res. 36 (2022) 2127-2142. https://doi.org/10.1002/ptr.7433.

[77] Y. Fan, S. Li, X. Ding, et al., First-in-class immune-modulating small molecule Icaritin in advanced hepatocellular carcinoma: preliminary results of safety, durable survival and immune biomarkers, BMC Cancer. 19 (2019) 279. https://doi.org/10.1186/s12885-019-5471-1.

[78] G.-R. Li, G.-Y. Xia, L.-N. Zhou, et al., Albiflorin: a promising natural monoterpene glycoside with potential therapeutic benefits for multiple physiological systems, Food & Medicine Homology. (2025) https://doi.org/10.26599/FMH.2025.9420064.